Russian Chemical Reviews **80** (12) 1139 – 1158 (2011) © 2011 Russian Academy of Sciences and Turpion Ltd

DOI 10.1070/RC2011v080n12ABEH004240

Semiconductor nanoparticles with spatial separation of charge carriers: synthesis and optical properties

R B Vasiliev, D N Dirin, A M Gaskov

Contents

I.	Introduction	1139
II.	The quantum size effects, electronic structure and optical properties of semiconductor nanoparticles	1140
III.	Peculiarities of the electronic structure and optical properties of core/shell semiconductor nanoparticles	1143
IV.	Methods of synthesis of core/shell semiconductor nanoparticles	1150
V.	Anisotropic nanoparticles with semiconductor/semiconductor heterojunctions	1152
VI.	Conclusion	1156

Abstract. The results of studies on core/shell semiconductor nanoparticles with spatial separation of photoexcited charge carriers are analyzed and generalized. Peculiarities of the electronic properties of semiconductor/semiconductor heterojunctions formed inside such particles are considered. Data on the effect of spatial separation of charge carriers on the optical properties of nanoparticles including spectral shifts of the exciton bands, absorption coefficients and electron – hole pair recombination times are presented. Methods of synthesis of core/shell semiconductor nanoparticles in solutions are discussed. Specific features of the optical properties of anisotropic semiconductor nanoparticles with the semiconductor/semiconductor junctions are noted. The bibliography includes 165 references.

I. Introduction

Progress in the design of new nanomaterials with specified properties is to a great extent due to the advances in the development of new synthetic approaches to nanoparticles including semiconductor nanoparticles that attract considerable attention of researchers. The quantum size effects in particles whose size is smaller than the Bohr exciton radius are basic to the electronic and optical properties of semiconductor nanoparticles.[1] Usually, such particles are 2 to 10 nm in size and comprise 10^3 to 10^5 atoms. In some cases, nanoparticles are stabilized by organic ligands attached to the nanoparticle surface. Ligand-stabilized semiconductor nanoparticles can be obtained by solution-phase chemical synthesis. A feature of these nanoparticles is that they can form stable sols in nonpolar solvents. Chemical methods of synthesis do not require expensive vacuum apparatus and the necessary amounts of nanoparticles can be obtained with ease. The fact that the optical properties depend on the nanoparticle size offers prospects for the design of new-generation solar cells, lasers, light-emitting diodes, luminescent labels and photocatalysts based on nanoparticles.[2 – 5]

In the present review, we consider a new class of nanoparticles based on semiconductor/semiconductor heterojunctions formed inside nanoparticles. In this case, a nanoparticle comprises two (and more) different-type semiconductor fragments that are, as a rule, epitaxially joined along particular crystallographic planes. An example is provided by well-known and well documented core/shell semiconductor nanoparticles in which a core is covered with a shell made of a wider bandgap semiconductor.[6] Such a structure allows the luminescence efficiency to increase due to passivation of surface defects. Core/shell nanoparticles with spatial separation of photoexcited charge carriers represent yet another example. Here, a feature of the electronic structure of the semiconductor heterojunction is that the energetically favourable arrangement of electrons and holes corresponds to their localization in different parts of a nanoparticle. Spatial separation of charge carriers was demonstrated for CdTe/CdSe nanoparticles as an example.[7] By varying the nanoparticle size one can control the charge separation processes and modify the optical properties, namely, to control not only the spectral position of an optical transition, but also the recombination times and the extinction coefficients.[8] Moreover, modern synthetic approaches allow one to obtain anisotropic nanoparticles with a specified shape; this extends the possibilities for control of their properties.

Due to their nanoscale size, semiconductor nanoparticles with spatial separation of charge carriers have a discrete electronic structure. They occupy an intermediate position between semiconductor heterostructures[9] and charge-transfer molecular complexes (Fig. 1).[10]

R B Vasiliev, D N Dirin, A M Gaskov Department of Materials Science and Department of Chemistry, M V Lomonosov Moscow State University, Leninskie Gory 1, 119991 Moscow, Russian Federation.
Fax (7-495) 939 09 98, tel. (7-495) 939 54 71,
e-mail: romvas@inorg.chem.msu.ru, romvasiliev@rambler.ru (R B Vasiliev), ddirin@gmail.com (D N Dirin), gaskov@inorg.chem.msu.ru (A M Gaskov)

Received 22 June 2011
Uspekhi Khimii **80** (12) 1190 – 1210 (2011); translated by A M Raevskiy

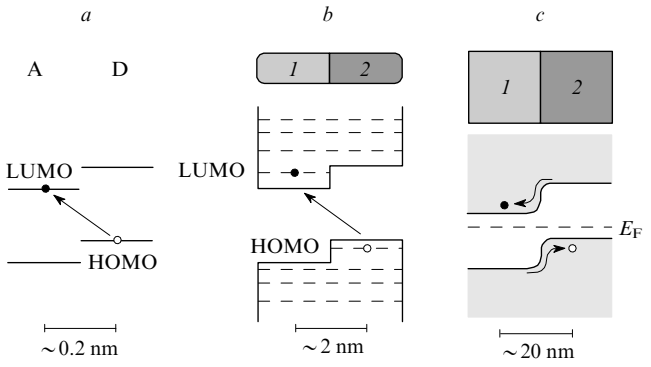


Figure 1. Electronic structure of charge-transfer complexes (*a*), semiconductor nanoparticles with spatial separation of charge carriers (*b*) and semiconductor heterostructures (*c*).
A is acceptor and D is donor; filled circles denote electrons and open circles denote holes; '*1*' denotes a semiconductor with higher electron affinity, '*2*' denotes a semiconductor with lower electron affinity; E_F is the Fermi level, LUMO denotes the lowest unoccupied molecular orbital and HOMO denotes the highest occupied molecular orbital. Arrows denote the direction of charge transfer upon photoexcitation; the characteristic sizes of charge-transfer regions are listed below.

Recently, the number of objects and approaches to the synthesis of nanoparticles with semiconductor/semiconductor heterojunctions have been extended significantly. A number of reviews devoted to this type of nanoparticles including semiconductor nanoparticles with spatial separation of charge carriers are available.[11–16] These publications are mainly focused on the synthetic aspects, morphology and crystal structure of nanoparticles with semiconductor/semiconductor [11–15] and metal/semiconductor heterojunctions;[16] the optical properties were described to a lesser extent.

In the present review we use the results of the studies carried out mainly in the last decade to analyze the peculiar features of the electronic structure of semiconductor nanoparticles with spatial separation of charge carriers, the dependence of their electronic structure on the type of heterojunction, on the particle size and morphology, and the effect of spatial separation of charge carriers on the optical properties of nanoparticles. We will consider methods of solution-phase synthesis, which allow one to obtain core/shell nanoparticles with highly homogeneous size and shape distribution, as well as anisotropic nanoparticles of specified shape.

II. The quantum size effects, electronic structure and optical properties of semiconductor nanoparticles

1. The quantum size effects in semiconductors

The quantum size effects in semiconductor nanoparticles were for the first time demonstrated and explained in the early 1980s by Ekimov [17] for nanoparticles in a glass matrix and by Brus [18] for nanoparticles in a sol. To that time, the quantum size effects in semiconductors were known for quasi-2D structures (quantum wells) comprising a thin epitaxial semiconductor film placed between layers of a wider bandgap material.[19] In quantum wells, charge carriers execute an in-plane motion and cannot move in the perpendicular direction. Analogously, charge carriers in quantum wires can move along one direction only.[20] In quantum dots, which are practically implemented in the form of semiconductor nanoparticles, charge carriers can not move along all spatial coordinates.[1,6] This leads to degeneration of a continuous energy spectrum to discrete energy levels. As the nanoparticle size and, correspondingly, the number of atoms in these levels increases, the energy gaps between the HOMO and LUMO decrease. Therefore, the energy of the HOMO–LUMO transition (analogue of the effective bandgap) depends on size of the nanocrystal, namely, it decreases down to the bandgap of bulk semiconductor as the nanocrystal size increases. A conditional threshold value of the nanoparticle size, which corresponds to the onset of size effects, is the Bohr exciton radius for a given material

$$a_B = a_0 \frac{\varepsilon m_0}{\mu}, \quad (1)$$

where a_0 is the first Bohr radius of hydrogen atom, ε is the dielectric constant of the semiconductor, m_0 is the rest mass of electron, μ is the reduced (effective) mass of exciton

$$\frac{1}{\mu} = \frac{1}{m_e} + \frac{1}{m_h},$$

m_e is the mass of electron and m_h is the mass of hole. If the nanoparticle radius r is such that $r < a_B$, the exciton energy is higher than the energy of a free exciton in the bulk material.[6,21]

The Bohr exciton radii of the $A^{II}B^{VI}$ and $A^{III}B^{V}$ semiconductors taken from Ref. 22 are listed in Table 1. For most substances, the Bohr exciton radii are of the order of the nanoparticle size (1–15 nm). Practically, this means the possibility to obtain nanoparticles with pronounced quan-

Table 1. Crystal structures of the $A^{II}B^{VI}$ and $A^{III}B^{V}$ semiconductors stable at room temperature, the corresponding lattice constants (*a*, *c*) and the Bohr exciton radii (a_B).

Semiconductor	Structural type	*a* /Å	*c* /Å	a_B /nm
MgSe	zinc-blende	5.9100	–	2.5
MgTe		6.4200	–	3.4
ZnO	wurtzite	3.2495	5.2069	2.6
ZnS		3.8226	6.2605	2.5
ZnSe	zinc-blende	5.6692	–	4.0
ZnTe		6.0090	–	5.0
CdS	wurtzite	4.1367	6.7161	4.1
CdSe		4.2999	7.0109	5.2
CdTe	zinc-blende	6.4810	–	6.8
AlN	wurtzite	3.1120	4.982	2.0
AlP	zinc-blende	5.4635	–	3.1
AlAs		5.6613	–	5.0
AlSb		6.1355	–	4.9
GaN	wurtzite	3.1896	5.1855	3.9
GaP	zinc-blende	5.4508	–	6.2
GaAs		5.6533	–	11.4
GaSb		6.0959	–	23.3
InN	wurtzite	3.5480	5.760	6.9
InP	zinc-blende	5.8690	–	9.6
InAs		6.0583	–	33.7
InSb		6.4793	–	72.5

tum size effects for all of these materials. The size-dependent properties of anisotropic nanoparticles are affected by the smaller dimension. For instance, a study of CdSe nanorods longer than 10–15 nm showed that variation of their length has little effect on the effective bandgap ($E_{g\,qd}$), whereas variation of the diameter causes $E_{g\,qd}$ to vary over a rather wide range.[23,24]

2. The electronic structure and optical properties

As the nanoparticle size decreases, the energy gaps between the size quantization levels of electron and hole increase. Under resonant excitation conditions (*e.g.*, absorption of a photon with appropriate energy), an electron goes from the highest occupied level (from the valence band) to the lowest unoccupied level (to the conduction band). The nomenclature of optical transitions is well documented.[25,26] For example, the lowest-lying optical transitions observed for spherical CdSe nanoparticles are as follows:[26] $1S_{3/2}(h)-1S(e)$, $2S_{3/2}(h)-1S(e)$, $1S_{1/2}(h)-1S(e)$, $2S_{1/2}(h)-1S(e)$ and $1P_{3/2}(h)-1P(e)$. In some cases, the order of transitions can change.[27] Complication of the morphology or composition of nanoparticles causes changes in the symmetry of electron–hole states and in the order of the corresponding transitions.[24,28,29] Electronic transitions between the size quantization levels are often called excitonic transitions.

The lowest-energy exciton maximum near the absorption edge in the absorption spectra of nanoparticles is detected most clearly and can serve as a source of information on the electronic structure of nanoparticles and on statistical characteristics of their ensemble.[29–33] The energy of the first exciton maximum (effective bandgap) is first of all determined by the nanoparticle material and size (d) and, ignoring small electrostatic corrections, can be estimated as

$$E_{g\,qd} = E_g + \frac{2\pi\hbar^2}{\mu d^2}, \qquad (2)$$

where E_g is the bandgap of the bulk semiconductor.[34]

Thus, as the nanoparticle size decreases, the effective bandgap increases approximately as d^{-2}. By using different materials and varying the nanoparticle size one can prepare nanoparticles with effective bandgaps lying between nearly 0.5 and 3.5–4 eV (Fig. 2). This makes it possible to span the wavelength range from the IR to near-UV region.

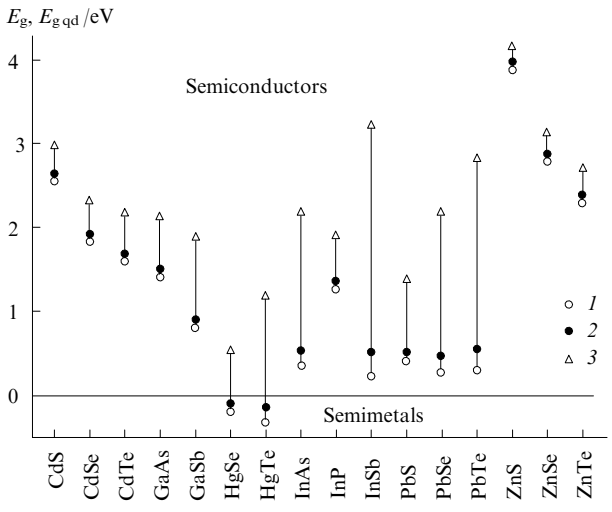


Figure 2. Effective bandgaps of various semiconductor nanoparticles of different size.[29]
Bulk material (*1*), 10-nm nanocrystal (*2*) and 3-nm nanocrystal (*3*).

When choosing an appropriate method of synthesis, it is of great importance to establish correlations between the nanoparticle size and spectral characteristics, *viz.*, spectral positions of exciton absorption and luminescence bands, extinction coefficients and absorption band widths.

Generally, the experimental dependence of the position of the exciton absorption band on the nanoparticle size obeys expression (2). In practice, one deals with approximation of the experimental dependences of the wavelength of the first exciton maximum on the nanoparticle size, as was done for spherical cadmium chalcogenide nanocrystals[30] (Fig. 3). Analogous experimental dependences are also available for CdTe,[35] InP,[36] CdSe,[37] CdS[38] and InAs.[39] It should be noted that the dependences reported by different authors[30,37] are in reasonable agreement with each other and confirmed by the results of theoretical calculations by the semiempirical pseudopotential method. Using the plots shown in Fig. 3, the average diameter of nanoparticles in an ensemble can be determined from optical absorption data with high accuracy.

Photoexcitation of a nanoparticle can be followed by nonresonant, resonant or intraband optical transitions

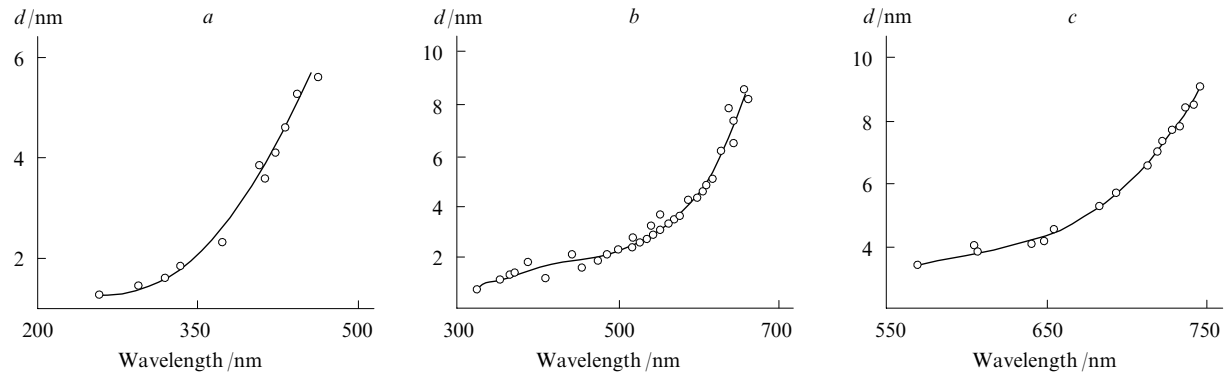


Figure 3. The wavelength of the first exciton absorption maximum plotted *vs.* size of spherical nanoparticles: CdS (*a*), CdSe (*b*), CdTe (*c*).[30]

corresponding to energies higher than, equal to or lower than the effective bandgap. Optical absorption spectroscopy is the most widely used method of analysis of the size effects in semiconductor nanoparticles. However, transitions between the size quantization levels in the absorption spectrum are often insufficiently well-resolved due to inhomogeneous broadening caused by the particle size and shape distribution and by different-type localization of surface defects. More detailed investigations of these transitions are carried out using various methods including luminescence excitation spectroscopy, time-resolved differential absorption spectroscopy and photoluminescence line narrowing spectroscopy.[25]

Dispersion of nanoparticle parameters (*e.g.*, the concentration of surface defects) can influence the density of states function, which in turn leads to changes in the band overlaps in the spectrum and result in the broadening of the absorption bands.[25] This is particularly pronounced in the high-energy region where the density of states is higher. For example, for a series of CdSe nanoparticles of different size, discrete bands appear in the absorption spectra within about 1 eV on the high-energy side of the first optical transition $[1S_{3/2}(\mathrm{h}) - 1S(\mathrm{e})]$. At higher energies, discrete optical transitions merge into a structureless absorption 'tail'.[32]

The extinction coefficient is an important optical characteristic. A decrease in the intensity of radiation that has passed through a sample is due to its absorption (C_{abs}) and scattering (C_{scat}). Since the nanoparticle size is much smaller than the wavelength of incident radiation, C_{scat} is much smaller than C_{abs} and scattering can be ignored.[40] The absorption of an ensemble of nanoparticles at the electronic transition wavelength is related to the oscillator strength f_{ij} of this transition and the number of unit ion pairs

$$\varepsilon \sim \sigma \sim \mu V_{\mathrm{qd}} \,. \tag{3}$$

where ε is the extinction coefficient of nanoparticles, σ is the effective absorption cross section of one structural unit of the semiconductor ($\mu \sim f_{ij}$) and V_{qd} is the nanoparticle volume.[33]

The experimentally determined dependences of the extinction coefficients ($\varepsilon_{\mathrm{ex}}$) at the first exciton maximum on the size of cadmium chalcogenide nanoparticles are shown in Fig. 4. The extinction coefficient increases as the particle size increases. This is first of all due to an increase in the effective absorption cross section. The molar extinction coefficient of spherical nanoparticles is related to the particle size as follows:[30, 31]

$$\varepsilon \sim d^{b},$$

where b changes from 2 to 3.

The extinction coefficients of the first exciton maximum of CdSe nanoparticles are also available in the literature.[33, 37, 41–43] The results [30, 31, 33] are in reasonable agreement with one another, but at small particle sizes they are somewhat different from the results of another study.[37] The results of theoretical calculations of the extinction coefficient [37] agree well with the experimental results.

At high energies, an increase in the electron and hole density of states causes the absorption spectrum of semiconductor nanoparticles to merge into a structureless absorption identical for all samples irrespective of the particle size. The shape of the absorption spectra of CdSe nanoparticles at photon energies higher than 3.5 eV matches that of the absorption spectrum of bulk semiconductor corrected for the local field effects.[32] This suggests that at high energies, the absorption of nanoparticle sols is solely determined by the volume fraction of the semiconductor material. Taking into account this fact, the extinction coefficients and the effective absorption cross section per unit ion pair were calculated for CdTe and CdSe.[33] At a photon energy of 3.1 eV, the effective absorption cross section per unit ion pair at a photon energy of 3.1 eV is

$$\mu_{3.1} = \frac{n_{\mathrm{sem}}}{n_{\mathrm{solv}}} |F_{\mathrm{loc}}|^2 \frac{\alpha_{3.1}}{N_{\mathrm{unit}}} \,, \tag{4}$$

where n_{sem} and n_{solv} are the real parts of the refractive index of the semiconductor and solvent, respectively; $|F_{\mathrm{loc}}|^2$ is the correction for the local field effects, $\alpha_{3.1}$ is the bulk absorption coefficient of the semiconductor at a photon energy of 3.1 eV; and N_{unit} is the number of formula units per cubic centimetre. The F_{loc} value is given by

$$F_{\mathrm{loc}} = \frac{3m_{\mathrm{solv}}^2}{m_{\mathrm{sem}}^2 + 2m_{\mathrm{solv}}^2} \,, \tag{5}$$

where m_{sem} and m_{solv} are the complex refractive indices of the semiconductor and solvent, respectively. These parameters for CdTe, CdSe and CdS are listed in Table 2.

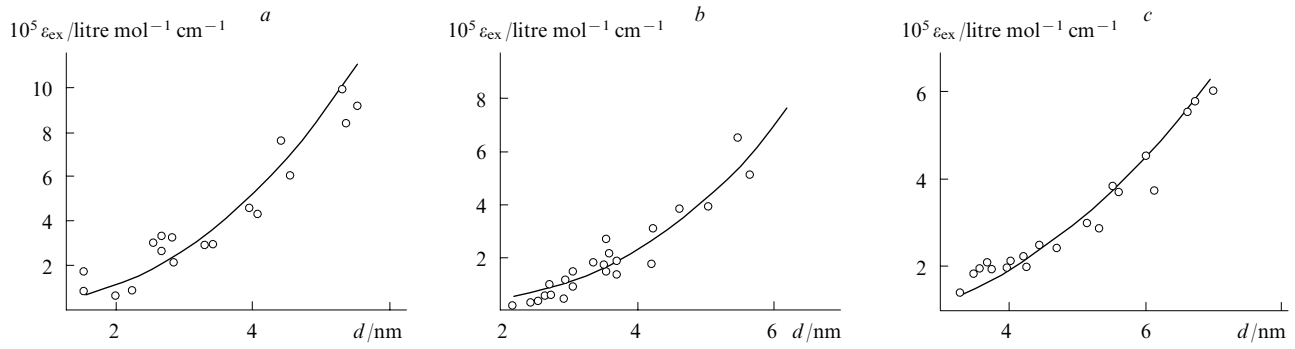


Figure 4. Experimental dependences of the extinction coefficients at the first exciton maxima on the size of spherical nanoparticles: CdS (*a*), CdSe (*b*), CdTe (*c*).[30, 31]

Table 2. Main optical constants of cadmium chalcogenides.[44–47]

Compound	n_{sem}	m^2_{sem}	F_{loc}	$10^5\,\alpha_{3.1}$ / cm^{-1}	$10^{-22}\,v$ /cm^3	z
CdTe	3.5	13.1	0.337	3	2.723	4 (cubic)
					1.336 (calculations)	2 (hexagonal)
CdSe	2.8	8.2	0.473	2	2.217	4 (cubic)
					1.123	2 (hexagonal)
CdS	2.6	6.9	0.530	1.4	1.969	4 (cubic)
					0.995	2 (hexagonal)

Note. The F_{loc} values are calculated using expression (5) for a spherical nanoparticle in hexane; v is the unit cell volume,[47] and z is the number of formula units per unit cell.

Typical solvents for nanoparticles stabilized by long-chain molecules include hexane (n_{solv} = 1.37486) and toluene (n_{solv} = 1.49693). They do not absorb in the region near 3.1 eV and therefore it can be assumed that $m_{solv} = n_{solv}$.

The corresponding extinction coefficient at a photon energy of 3.1 eV is

$$\varepsilon_{3.1} = \frac{n_{sem}}{n_{solv}} |F_{loc}|^2 \frac{\alpha_{3.1} N_A}{2303} V_{qd} \qquad (6)$$

and depends only on the optical parameters of the semiconductor and solvent and on the parameter V_{qd} (N_A is the Avogadro constant).

The so-called inhomogeneous broadening of an absorption band is mainly governed by the particle size distribution.[33] Homogeneous broadening is mainly due to electron–phonon interaction. The width of a homogeneously broadened absorption or luminescence band is much smaller than that observed in the experiment.[48,49] Assuming a Gaussian particle size distribution for the ith electronic transition, the inhomogeneous broadening (Γ_i) is proportional to the size dispersion $\delta_r = \Delta_r/r$ (Ref. 32)

$$\Gamma_i = 2\frac{\Delta_r}{r}\left(\hbar\omega_i - E_g\right) = 2\delta_r \Delta_i\,, \qquad (7)$$

where

$$\Delta_i = \hbar\omega_i - E_g\,,$$

$\hbar\omega_i$ is the energy of the ith transition, E_g is the bandgap of the bulk material and r is the particle radius. The absorption band width at half-height is $\Gamma_i 2\sqrt{2\ln 2}$.

Thus, the bands corresponding to higher-energy transitions are more broadened. The structureless absorption of the semiconductor, which matches its bulk absorption, is stronger in the UV region; therefore, positions of electronic transitions in this spectral region are difficult to determine. The effect of the structureless bulk absorption can be to some extent levelled by differentiating the absorption spectrum; this leads to an increase in the number of reliably observed bands and better determination of their spectral positions.[50]

III. Peculiarities of the electronic structure and optical properties of core/shell semiconductor nanoparticles

1. Heterojunctions in semiconductor structures

A semiconductor heterojunction is a contact between two different semiconductors. The main characteristic of a heterojunction is the energy band discontinuity at the junction. Usually, it is assumed that an abrupt transition from one semiconductor to the other occurs at a distance of at most a few lattice constants; consequently, to a first approximation, the energy band structure at the junction changes jumpwise.[9,51]

There are the following types of heterojunctions with respect to the sign and magnitude of the energy band discontinuity (Fig. 5):[51,52]

— type I heterojunction (see Fig. 5 *a*) is a straddling gap heterojunction formed by a wide-gap and a narrow-gap semiconductors; the conduction band offset and the valence band offset have different signs; the energetically favourable situation corresponds to both electron and hole localization in the same region of the heterostructure, *viz*., the narrow-gap semiconductor; examples are provided by the GaAs/AlAs and CdSe/ZnS systems;

— type II heterojunction (see Fig. 5 *b*) is a staggered gap heterojunction formed by two semiconductors with comparable bandgaps; the energy band offset have the same sign; the energetically favourable situation corresponds to spatial separation of charge carriers (localization of electron and hole in different regions of the heterostructure); examples

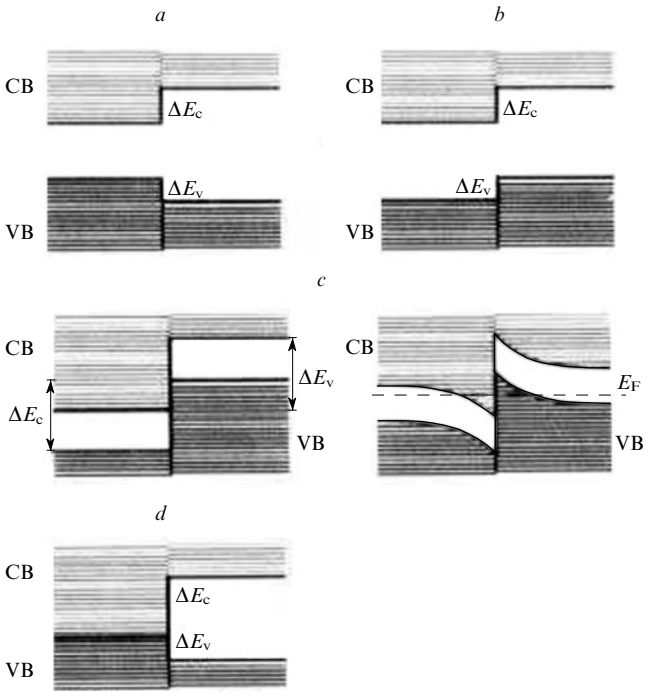


Figure 5. Energy band structures of different types of heterojunctions.[51]
(*a*–*d*) See text; CB is the conduction band, VB is the valence band, ΔE_c is the conduction band offset and ΔE_v is the valence band offset.

Table 3. Main parameters of the electronic structure of cadmium chalcogenides at the Γ point of the Brillouin zone.[22]

Material	Structural type	E_g /eV	Δ_{so} /meV	Δ_{cr} /meV	χ_c /eV	m_e/m_0	m_{hh}/m_0	m_{lh}/m_0	m_{so}/m_0
CdS	zinc-blende	2.46	70	–	–	0.14	0.68	0.15	0.24
CdS	wurtzite	2.501	65	28	4.5	0.151	0.66 [a]	–	–
CdSe	zinc-blende	1.675	410	–	–	0.119	0.57	0.11	0.18
CdSe	wurtzite	1.751	420	40	4.95	0.125	0.46 [b]	–	–
				–	4.78 [b]				
CdTe	zinc-blende	1.51	900	–	4.28	0.090	0.82	0.145	0.24
				–	4.18 [a]				

Note. Notations are as follows: Δ_{so} is the spin – orbit splitting; Δ_{cr} is the splitting of the Γ_8 subband in the wurtzite crystal field; m_e is the effective mass of electron; m_{hh}, m_{lh} and m_{so} are the effective masses of heavy, light and spin – orbit holes, respectively; and m_0 is the rest mass of electron. [a] Calculated using the Luttinger parameters. [b] According to Ref. 53.

are provided by the GaInAs/GaAsSb and CdTe/CdSe systems;

— type III heterojunction (see Fig. 5 *c*) is characterized, similarly to the type II heterojunction, by energy band offset of the same sign, but their absolute values are larger and the bands do not overlap; an example is provided by the InAs/GaSb system; and

— type IV heterojunction (see Fig. 5 *d*) is formed by a zero-gap semiconductor and a finite-gap semiconductor; an example is provided by the HgTe/CdTe system.

It should be noted that type III and type IV heterojunctions are realized for a few materials; corresponding data for core/shell nanoparticles are unavailable in the literature.

To a first approximation, band edges have constant positions.[51] The position of the bottom of the conduction band of a semiconductor on the energy scale is characterized by the electron affinity (χ_c).[53] The published χ_c values for the $A^{II}B^{VI}$ and $A^{III}B^{V}$ semiconductors vary over a wide range. Table 3 lists the most reliable χ_c values obtained by X-ray photoelectron spectroscopy. Mutual position of the band edges for some semiconductors is shown in Fig. 6. The conduction band offset at the heterojunction can be calculated as the electron affinity differences between the semiconductors. The valence band offset can be defined as the sum

$$\Delta E_v = \Delta E_c + \Delta E_g . \quad (8)$$

In real systems, one deals with redistribution rather than linear superposition of bulk quasi-atomic charges and potentials near the junction. Charge redistribution is a result of tunnelling, the action of image forces, *etc*.[9] These rearrangements induce an electronic dipole in the near-junction region, which shifts the bands relative to each other and relative to the bands in the linear superposition model.[9, 51] In addition to electronic dipoles one can expect the appearance of atomic (or ionic) interfacial dipoles if, for some reason, atoms of one semiconductor will cross the ideal junction and penetrate into the other semiconductor. Thus, estimation of energy band offsets is a particular task.

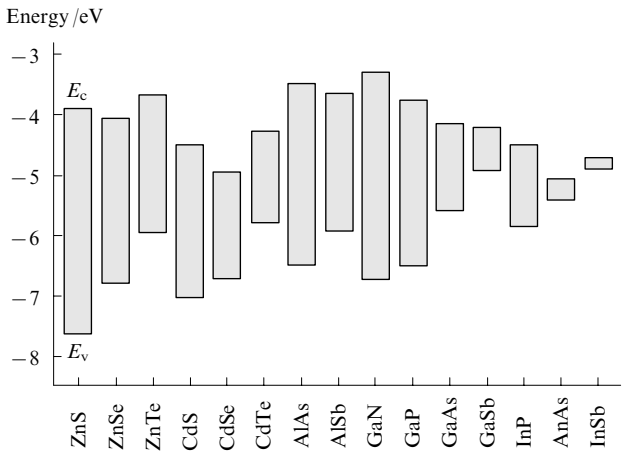


Figure 6. Diagram illustrating the mutual position of the conduction and valence band edges for $A^{II}B^{VI}$ and $A^{III}B^{V}$ semiconductors (data taken from Ref. 22).
E_v and E_c are the valence and conduction band edges, respectively.

2. The electronic structure of core/shell semiconductor nanoparticles

Studies of core/shell semiconductor nanoparticles also involve consideration of heterojunctions with corresponding (type I or type II) spatial localization of charge carriers (Fig. 7). The type of localization of charge carriers is specified by the positions of the size quantization levels. For bulk heterostructures, the localization region of charge carriers is always known with certainty. Namely, charge carriers are localized in the same region in type I heterojunctions and on different sides of the junction in type II heterojunctions. However, in nanosystems one deals with the quantum size effects and spatial localization of charge carriers depends on the size of the nanostructure. For instance, both types of charge carriers can be delocalized over the entire nanoparticle (no spatial separation) provided a type II heterojunction (so-called type I localization).[54] The reverse situation is also possible, where one type of charge carriers is spatially localized while the other type of charge carriers is delocalized over the entire nanoparticle provided a type I heterojunction (so-called type II localization).

Thus, the type of spatial localization of charge carriers can be controlled by varying the size of the core or shell. The localization regimes are illustrated by a scheme shown in Fig. 8. The smallest (largest) nanoparticle sizes correspond to type I (type II) localization. At intermediate nanoparticle sizes, one deals with quasi-type II localization, *viz*., one type of charge carriers is spatially localized while the other one is delocalized over the whole nanoparticle.

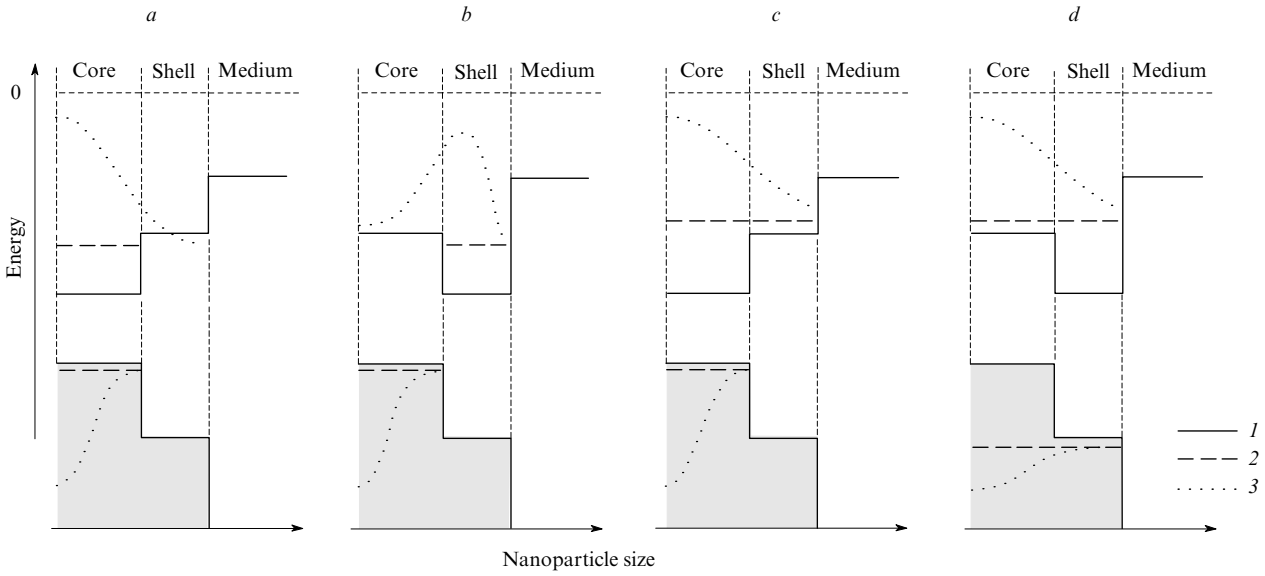


Figure 7. Localization of charge carriers for core/shell nanoparticles with type I (*a*, *c*) and type II (*b*, *d*) heterojunctions.
Conduction band (top) and valence band (bottom) edges (*1*), size-quantized levels of electron and hole (*2*) and the corresponding wave functions of charge carriers (*3*).

An interesting example of control of localization is provided by the so-called inverted nanoparticles in which a core of a wide-gap semiconductor is coated with a shell of a narrower-gap material.[54, 56, 57] As was shown in Fig. 9 for ZnSe/CdSe nanoparticles, both electron and hole are delocalized over the entire nanoparticle if the CdSe shell is sufficiently thin (Fig. 9 *a*). As the shell thickness increases, the electron and hole become spatially separated (Fig. 9 *b*) and then again localized in the same region (now within the CdSe shell, Fig. 9 *c*); *i.e.*, the localization type of charge carriers changes.

Therefore, the electronic properties of a nanoparticle are governed by the mutual position of the energy band edges at the heterojunction (see Fig. 6 and, *e.g.*, Ref. 58) and the nanoparticle size. Mutual position of the conduction and valence band edges for some semiconductor materials is shown in Fig. 6.

Considering the synthesis of core/shell nanoparticles, an important role is played by the possibility of creation of an abrupt heterojunction and epitaxial growth of components of the nanoparticle. This possibility is determined by the crystal lattice mismatch and by the solubility of components. Often, components of bulk semiconductors $A^{II}B^{VI}$ and $A^{III}B^{V}$ are mutually soluble.[59] For instance, both components of the CdS/CdSe system show an infinite

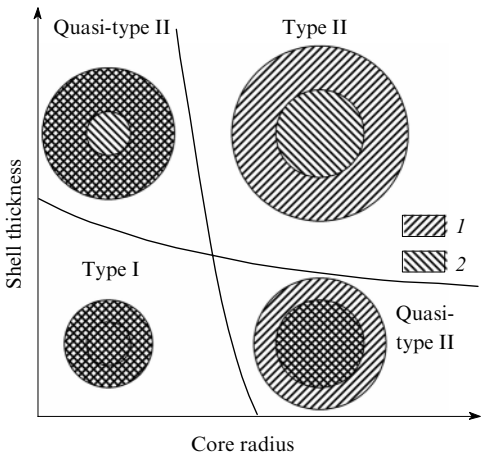


Figure 8. Spatial localization of charge carriers in a core/shell nanoparticle with type II heterojunction depending on the core and shell size.[8, 55]
Electron (*1*) and hole (*2*). Lines denote conditional boundaries that separate regimes with different types of spatial localization of charge carriers.

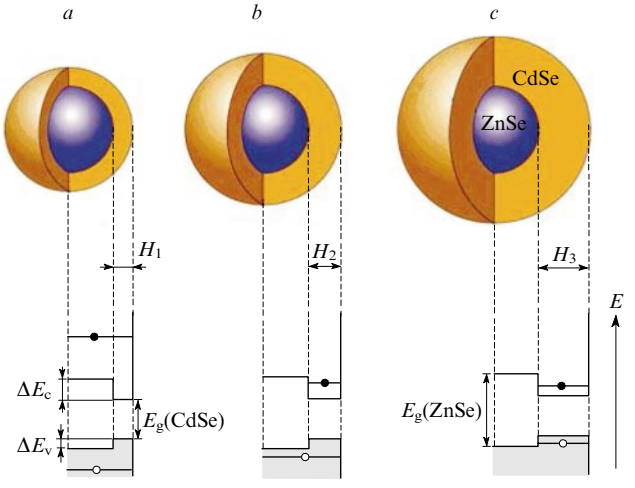


Figure 9. Change of the type of spatial localization of charge carriers with an increase in the shell thickness in ZnSe/CdSe nanoparticles.[54]
Type I, core/core (*a*); type II, shell/core (*b*); and type I shell/shell (*c*); $H_1 < H_2 < H_3$.

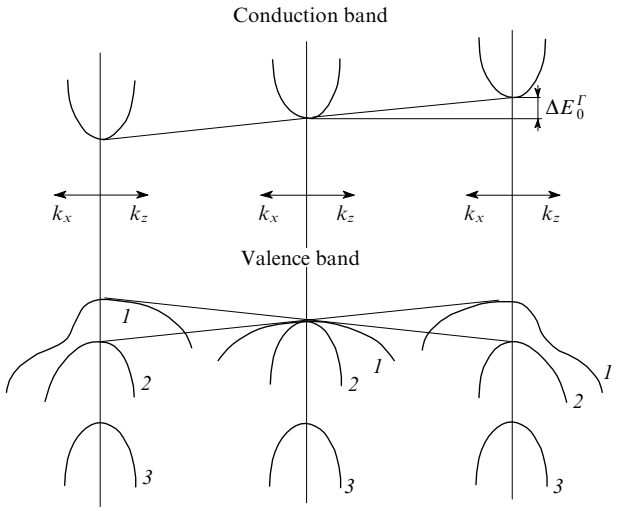


Figure 10. Influence of deformations on the energy band structure of sphalerite near the Γ point of the Brillouine zone.[22]
Heavy hole (*1*), light hole (*2*) and spin – orbit split-off hole (*1*); ΔE_0^Γ is the deformation-induced shift of the conduction band edge.

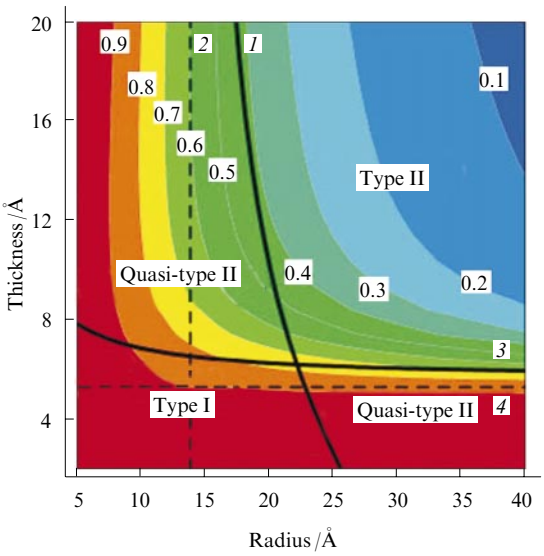


Figure 12. Theoretical dependences of θ^2 on the core radius and shell thickness for core/shell nanoparticles. Localization of charge carriers: electron (core)/hole (shell).[10]
(*1*–*4*) See text; numbers denote the θ^2 values.

mutual solubility, the ionic radii of sulfur (0.182 nm) and selenium (0.193 nm) differ insignificantly and E_g is a linear function of the composition.[60] The CdS/CdTe system is characterized by partial solubility of components and the ionic radii of tellurium (0.211 nm) and sulfur differ considerably. In this case, one deals with the so-called 'band sagging' effect.[61] In the CdTe/CdSe system, in spite of unlimited mutual solubility of the components, the difference between the ionic radii of selenium and tellurium is large enough and has strong effect on the character of the compositional dependence of the bandgap which shows a nonlinear behaviour.[59]

When choosing substances for the synthesis of core/shell nanoparticles, one of the most important factors is to have components with close values of lattice constants. An empirical rule is that the lattice constants of the core and shell materials should differ by at most 10% (see Table 2). Lattice mismatch at the heterojunction inevitably leads to mechanical deformations which penetrate into the interior of the nanoparticle by a few lattice constants and can therefore produce a strong effect. Methods of calculations

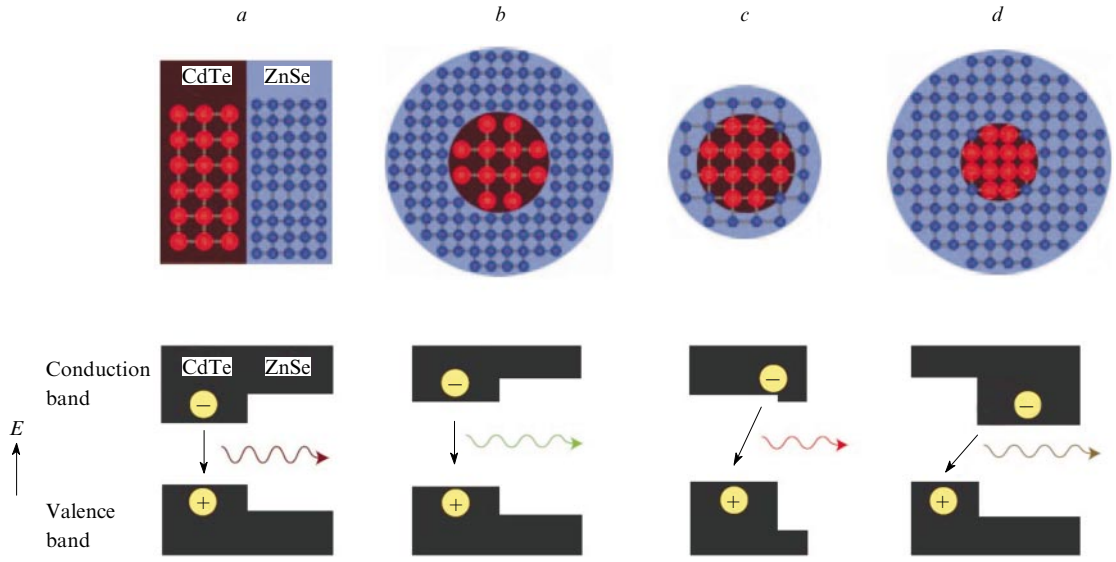


Figure 11. Lattice strain-induced changes in heterojunctions in the CdTe/ZnSe system.[72]
Bulk heterostructure (*a*), unstrained core/shell particle (*b*), thin epitaxial shell (*c*) and thick epitaxial shell (*d*). The colour of the wiggly arrows indicates the luminescence wavelength. The unstrained core/shell nanoparticle has a conventional type I heterojunction which changes to type II heterojunction upon compression of the core and stretching of the shell.

of deformations in nanostructures due to lattice constant mismatch have been documented.[62–67]

Mechanical strain in the system cause the conduction and valence band edges to shift.[22] Taking zinc-blende as an example, Fig. 10 illustrates the effect of mechanical strain on positions of the conduction and valence band edges. Usually, only small deformations are considered; here, the energy shift ΔE_0^{Γ} is a linear function of deformation. The coefficients of proportionality in these dependences (deformation potentials) for some semiconductors $A^{II}B^{VI}$ $A^{III}B^{V}$ were reported in the literature.[68–71] For most semiconductors, they are negative, *i.e.*, compression (stretching) of a crystal leads to an increase (decrease) in the conduction band edge energy level.

The influence of the lattice constant mismatch on the electronic structure of core/shell nanoparticles was studied.[72–74] Lattice strain can induce significant changes in the energy gap width in the case of epitaxial growth of the shell on a small compressed core (Fig. 11). A bulk CdTe/ZnSe system is characterized by a type I heterojunction and localization of both charge carriers in the CdTe region. However, epitaxial growth of the ZnSe shell leads to pronounced compression of the CdTe core because the CdTe lattice constant (6.481 Å) is much larger than that of the ZnSe lattice (5.669 Å). Compression of the core is accompanied by a decrease in the energy of the bottom of the conduction band; correspondingly, stretching of the shell causes this energy to increase (see Fig. 11). The two opposite effects lead to a change of the heterojunction type and a decrease in the effective bandgap.

Deformations of core/shell nanoparticles mainly occur in the core region.[72] Lattice compression by a few per cent produces changes in the electronic structure of a material by tens and even hundreds of meV according to the deformation potential.

3. Separation of charge carriers in core/shell nanoparticles

Quantitative estimation of spatial separation of charge carriers in core/shell nanoparticles is performed using the overlap integral (θ^2) of the electron and hole wavefunctions ψ_e and ψ_h, respectively, in spherical system of coordinates[8]

$$\theta^2 = \left(\int_0^{\infty} \psi_e(r)\psi_h(r) 4\pi r^2 \mathrm{d}r \right)^2 . \qquad (9)$$

The dependence of θ^2 on the core radius and on the shell thickness for a model semiconductor nanoparticle with an electron (core)/hole (shell) charge carrier localization type is shown in Fig. 12. An example is provided by the CdSe/CdTe nanoparticle.

Line *1* separates the regimes with electron delocalization over the whole nanoparticle (on the left of the line) and with electron localization in the core (on the right of the line); line *2* is the thick-shell asymptote; line *3* separates the regimes with hole delocalization over the whole nanoparticle (below the line) and with its localization in the shell (above this line); and line *4* is the thick-core asymptote. The smallest core and shell sizes correspond to type I localization regions, whereas the largest ones correspond to type II localization regions. Intermediate core and shell sizes are characterized by quasi-type II localization, *viz.*, one charge carrier is localized in some region of the nanoparticle while the other is delocalized over the nanoparticle.

4. The effect of separation of charge carriers on the optical properties of core/shell nanoparticles

Type II localization of charge carriers is accompanied by a decrease in the oscillator strength of the transition and in the effective bandgap and by emergence of electric field inside the nanoparticles. The first effect for ZnSe/CdSe nanoparticles is illustrated in Fig. 13 *a*. The overlap integral of the electron and hole wavefunctions determines the oscillator strength of the corresponding electronic transition. As θ^2 decreases, the electronic transition probability also decreases. As a result, an increase in the thickness of the CdSe shell causes an electron to move to the energetically favourable region within the shell. This manifests itself as a decrease in the absorption intensity of the first exciton maximum in the optical absorption spectra of ZnSe/CdSe nanoparticles (see Fig. 13 *a*). A rather strong exciton band in the absorption spectra of individual cores is transformed to a structureless absorption 'tail'. Further increase in the shell thickness is accompanied by motion of the second charge carrier (hole) to the shell, and the overlap integral increases. Changes in the relative intensity of the exciton band for nanoparticles of different size are illustrated in Fig. 13 *b*. The exciton absorption in the region corresponding to type II localization is suppressed, whereas in the region corresponding to small and large shell thicknesses the absorption maximum is more pronounced.

An important consequence of spatial separation of charge carriers in nanoparticles consists in the decrease in the probability of radiative recombination, which leads to an increase in the lifetime of photoexcited electron–hole pair (Fig. 14).[7, 56, 75] The probability of radiative recombination is proportional to the overlap integral of the electron and hole wavefunctions.[56] However, changes in the photoluminescence kinetics are often not limited to the increase in the lifetime. The probability of nonradiative recombination of an electron–hole pair with long lifetime is higher owing to the interaction with defect states. As a result, a larger number of states becomes involved in recombination.[76] In this case, the luminescence decay kinetics shows a complex multiexponential behaviour.[75]

As the shell thickness increases, the luminescence maximum is shifted towards the long-wavelength region due to a decrease in the effective bandgap for the space-indirect transition. The bandgap will be determined by the energy difference between the bottom of the conduction band of the material with the higher χ_c value and the top of the valence band of the material with the lower ionization energy; this allows energies lower than the bandgap of each constituent semiconductor to be attained. Note that spatial separation of charge carriers leads to changes not only in the exciton lifetimes and oscillator strengths, but also in the spectral positions of electronic transitions. This is due to the emergence of electric field inside the nanoparticles owing to the appearance of noncompensated charge regions. The embedded electric field will strongly affect the behaviour of multiexcitons in the nanoparticle.[8, 77] According to calculations, core/shell nanoparticles with spatial separation of charge carriers are characterized by positive energy of Coulomb interaction of a biexciton which can reach values of the order of 100 meV;[8] this is comparable with typical widths of optical bands. This is the reason for the situation where a large Coulomb shift of optical transitions in a singly excited nanoparticle leads to almost complete suppression of absorption at the lumines-

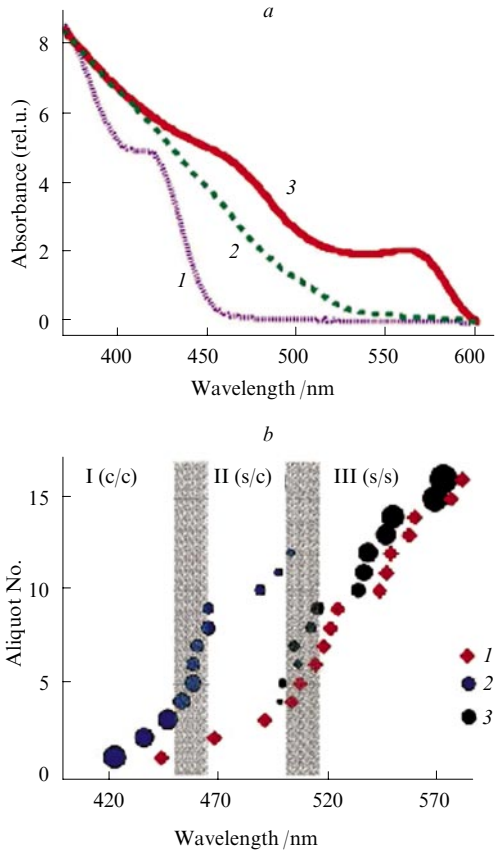


Figure 13. Absorption spectra of ZnSe/CdSe nanoparticles with a fixed core radius of 1.5 nm and three different thicknesses (H) of the shell (a)[57] and changes in positions of the photoluminescence maximum and minima of the second derivative of the absorption spectrum (b).[54]
(a) H_1 (1) < H_2 (2) < H_3 (3); (b) the sizes of the rhombi and circles denote the relative intensities of the exciton absorption band; changes in position of the photoluminescence maximum (1); and positions of the two first minima of the second derivative of the absorption spectrum corresponding to the maximum of the exciton absorption band (2, 3); nanoparticle type: I (c/c) — both charge carriers are located in the core; II (s/c) — one charge carrier is located in the shell, the other charge carrier located in the core; and I (s/s) — both charge carriers are located in the shell.

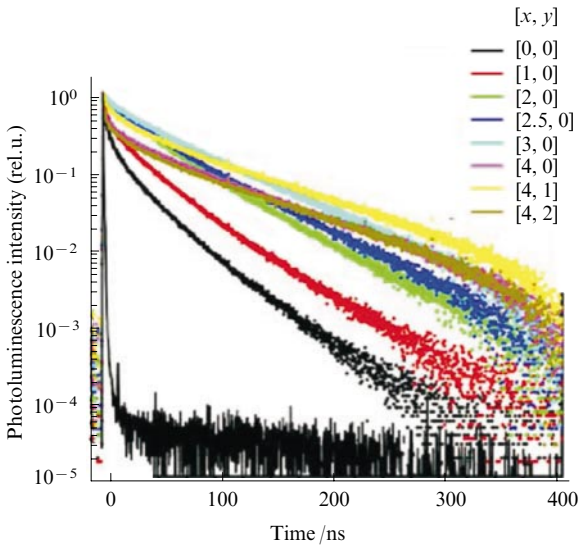


Figure 14. Photoluminescence kinetics of CdTe and CdTe/CdSe/CdS nanoparticles with different number of shell monolayers;[75] x and y denote the numbers of CdSe and CdS monolayers, respectively. The instrumental response function is shown in black.

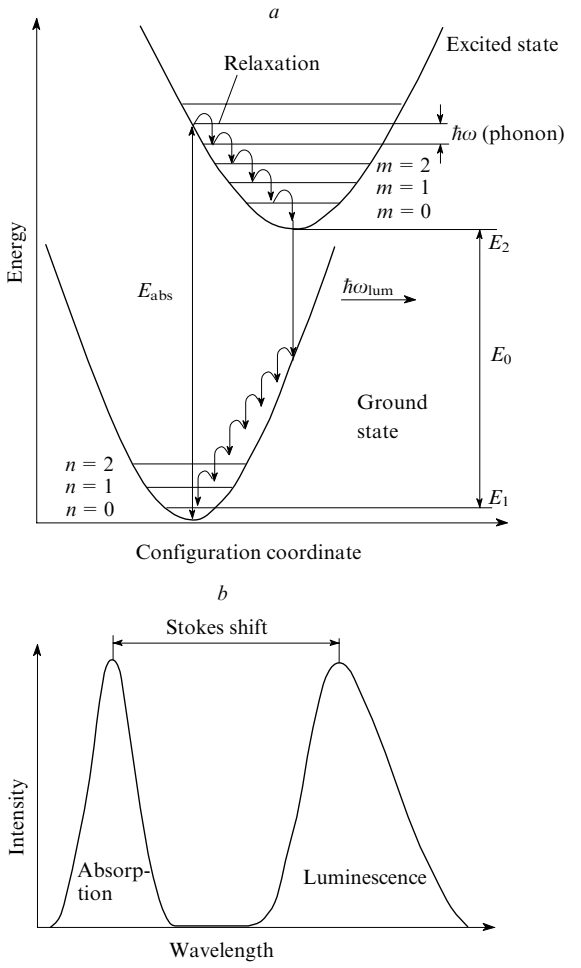


Figure 15. Schemes of electronic transitions for optical absorption and luminescence (a) and the corresponding spectral bands (b);[82] n, m are the numbers of vibrational levels in the ground and excited state, respectively.

cence wavelength. Under these conditions, stimulated emission can be attained even in the single-exciton regime, which allows one to avoid difficulties related to fast radiative recombination due to the Auger processes. This effect can be used in the design of quantum dot lasers. To date, spherical nanoparticles with type II heterojunction including CdTe/CdSe, CdTe/CdS, ZnSe/CdSe and CdS/ZnSe have been reported.[7, 56, 75, 78, 79]

As mentioned above, semiconductor nanoparticles with spatial separation of charge carriers are analogues of charge-transfer molecular complexes (see Fig. 1) and can therefore be considered from the standpoint of the Markus–Hush thermodynamic theory of charge transfer.[80, 81] Absorption of a photon causes a nanoparticle to undergo transition from the ground to excited state. The formation of an electron–hole pair should be accompanied by the electron density redistribution over the nanoparticle, which corresponds to different position of the ground- and

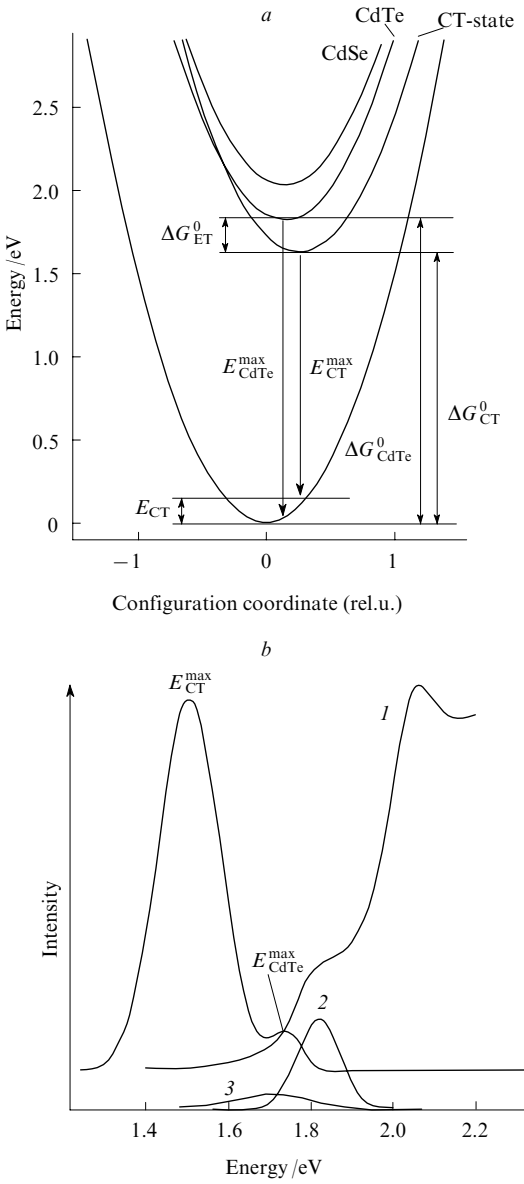


Figure 16. Free energy curves plotted in the configuration coordinates for CdTe/CdSe nanoparticles (*a*) and the corresponding absorption and luminescence spectra (*b*).[80]
(*a*) Changes in the free energy on charge transfer (ΔG^0_{ET}), excitation (ΔG^0_{CdTe}) and relaxation (ΔG^0_{CT}) of electron; E^{max}_{CdTe} and E^{max}_{CT} are the energies of the exciton luminescence band and the CT-band ; and E_{CT} is the reorganization energy of the medium upon charge transfer;
(*b*) the bands corresponding to the exciton absorption in CdSe (*1*) and CdTe (*2*) and to absorption of the CT-state (*3*).

excited-state minima on the energy diagram in the configuration coordinates (Fig. 15). Relaxation of electron to a lower-energy excited state can occur *via* vibrational levels through electron–phonon interaction.[82] Analogously, excited nanoparticles with spatial separation of charge carriers undergo transition to charge-transfer (CT) states followed by true relaxation (Fig. 16). Because of this, the absorption and luminescence spectra of nanoparticles with spatial separation of photoexcited charge carriers can exhibit both exciton and CT bands. The latter bands are usually weak in the absorption spectra due to the low probability of the corresponding electronic transition.[81, 83]

The emission energy is always somewhat lower than the absorption energy. In the case of monodisperse nanoparticles, the difference between these energies is called the resonant Stokes shift[80, 84] which increases as the nanoparticle size decreases (Fig. 17 *a*). The experimental dependence is in good agreement with the theoretical splitting between the 'dark' (spin-forbidden) and 'light' (spin-allowed) exciton states.[80]

Nonresonant Stokes shift observed for an ensemble of nanoparticles also increases with decreasing the nanoparticle size (Fig. 17 *b*). Its magnitude is to a great extent determined by the nanoparticle size dispersion.[80, 84] Moreover, the nonresonant Stokes shift is affected by the shape, structure and differences in the chemical environment of nanoparticles.[80, 84] For this reason, the experimentally determined Stokes shift does not always agree with the theoretical dependences.

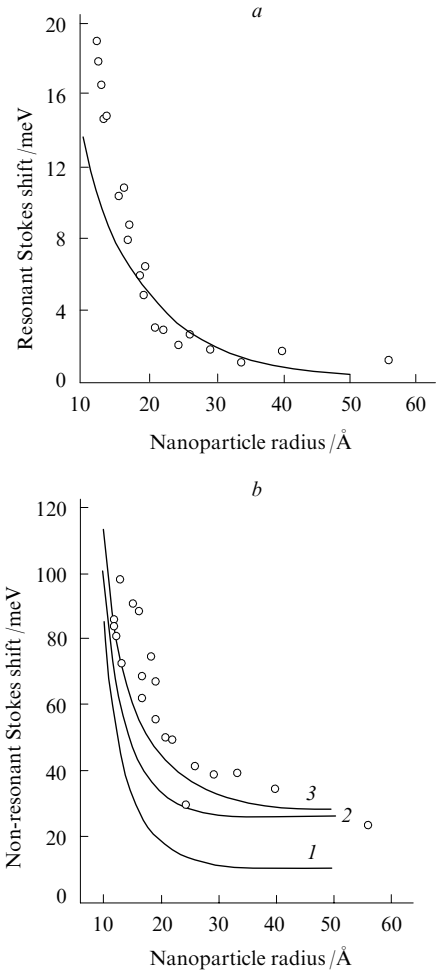


Figure 17. Resonant (*a*) and non-resonant (*b*) Stokes shifts plotted *vs*. CdSe nanoparticle size.[80, 84]
(*a*) Solid line denotes the theoretical dependence of the splitting between the 'dark' and 'light' exciton;
(*b*) theoretical dependence at a size dispersion of 5% (*1*), dependence plotted taking into account the phonon contribution to the Stokes shift (*2*), and theoretical dependence at a size dispersion of 10% (*3*).

IV. Methods of synthesis of core/shell semiconductor nanoparticles

1. The choice of initial reactants and stabilization of nanoparticles

To date, numerous methods of synthesis of semiconductor nanoparticles have been developed. Below we will consider chemical methods of synthesis in nonpolar solvents in the presence of stabilizers. Their advantages are as follows:[85–87]

— the possibility of control of nanoparticle growth,

— good passivation of the surface states of nanoparticles,

— narrow nanoparticle size distribution (scatter of the order of 5%–8%), and

— the possibility of subsequent isolation and purification of nanoparticles (no matrix).

The synthesis of semiconductor nanoparticles in solutions of tributylphosphine (TBP) and tributylphosphine oxide (TBPO) was proposed.[88] Using these compounds, one can control the nanoparticle growth and carry out the synthesis at a rather high temperature (namely, at 220 °C to provide the formation of a crystal structure with lower content of defects). Subsequently, the technique was modified[89] and the possibility of carrying out reproducible synthesis of highly monodisperse nanoparticles appeared.

As a rule, chemical methods involve a rapid introduction of initial reactants into a heated nonpolar solvent containing a stabilizer of nanoparticles. A rapid reaction occurs, resulting in the formation of a supersaturated solution and subsequent intense nucleation (Fig. 18). As the degree of supersaturation decreases, nucleation ceases and seeds continue to grow. Since the nucleation stage takes a short time, nanoparticles have a narrow size distribution. Yet another mechanism of reduction of the nanoparticle size dispersion possible at high supersaturations is called 'focusing' of size distribution.[90,91] It should be noted that the growth stage, when the reaction mixture is considerably depleted in initial reactants, can be followed by Ostwald ripening leading to an increase in polydispersity. The main approaches to control of nanoparticle size distribution have been reviewed.[92]

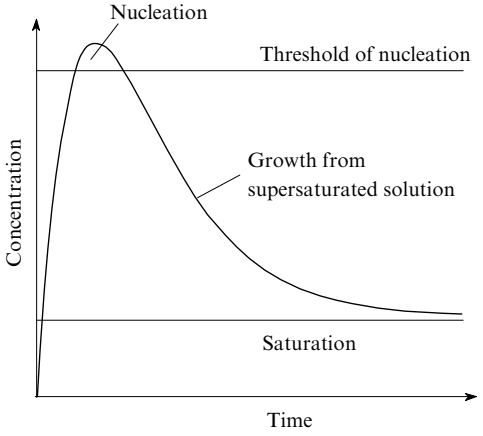


Figure 18. LaMer diagram of changes in the precursor concentration during nanoparticle growth.

Methods of synthesis in nonpolar solvents developed to date include the synthesis in a stabilizing solvent and the synthesis using stabilizing precursors.

In the former case, the stabilizing solvents usually include alkylphosphines, alkylphosphine oxides, alkyl phosphites, alkyl phosphates, pyridine, alkylamines and furan; trioctylphosphine oxide (TOPO) is most often used;[89] dimethyl cadmium is a possible source of cadmium.

In the latter case, inert solvents include, *e.g.*, diphenyl ether or octadecene; cadmium oleate can be used as both initial reactant and stabilizer.[93]

In the synthesis of $A^{II}B^{VI}$ semiconductor nanoparticles, cations can be supplied from metal alkyl derivatives and metal oxides or their organic salts. For example, possible sources of cadmium include CdO,[76,81,94–100] $Cd(OAc)_2$,[77,101–104] Me_2Cd[95,105–110] and other compounds. Group VI element anions can often be obtained using organic phosphine chalcogenides[94–110] or trimethylsilyl chalcogenides $(TMS)_2E$ (where E = S, Se, Te) as initial reactants.[89]

The synthesis of $A^{III}B^{V}$ semiconductor nanoparticles is somewhat different from the synthesis of the $A^{II}B^{VI}$ semiconductor nanoparticles.[111–113] First, the $A^{III}B^{V}$ semiconductors are characterized by higher covalency and therefore the formation of a crystal structure with low content of defects requires a higher temperature of the synthesis. This can lead to irreversible aggregation of particles. Second, the compound $A^{III}B^{V}$ cannot be obtained by solution-phase synthesis as a result of a direct reaction between corresponding atoms or ions (as for $A^{II}B^{VI}$) because they will react with the solvent. A way to solve this problem is to form complexes that prevent undesired reactions and produce the necessary compounds after pyrolysis. Most often, the synthesis is carried out in high-boiling stabilizing solvents using trimethylsilyl derivatives of Group V elements [$(TMS)_3P$, $(TMS)_3As$)][114–120] and anhydrous metal halides (*e.g.*, $InCl_3$) as sources of metals.[115,116,120] However, these compounds are characterized by low reactivities; correspondingly, the reaction time increases, which leads to polydisperse nanoparticles. These methods have been best developed to synthesize InP nanoparticles.[115,117–123]

Nanoparticles with a large proportion of surface atoms are thermodynamically unstable. They can be stabilized by introducing stabilizers of disperse systems. The proper choice of a stabilizer is basic to the synthesis of nanoparticles. Stabilizers should meet rather strict requirements:

— it should prevent aggregation rather than growth of nanoparticles;

— its molecules should form sufficiently strong bonds with the nanoparticle surface; and

— the stabilizer molecules should passivate the nanoparticle surface, thus saturating broken bonds that act as traps of charge carriers.

Structural, mechanical and electrostatic stabilization of nanoparticles has been studied in detail.[124] The range of potential organic stabilizers includes all nucleophilic reactants containing a group coordinating to the metal (usually, an electron-donating group) and long-chain substituents, *e.g.*, long-chain amines, thiols and higher carboxylic acids.[90] Each class of compounds is described in detail below.

Amines. The properties of amines depend on the degree of substitution at the nitrogen atom. Primary and secondary amines can act as electron-donating (with cadmium) or electron-withdrawing (with tellurium) centres. Owing to

these properties, amines can be used as stabilizers. Also, it is important that aliphatic amines are stronger nucleophiles compared to aromatic amines; this allows one to introduce long-chain hydrocarbon substituents.

Thiols are well soluble in many organic solvents and form strong S—M (M is a metal) bonds with the nanoparticle surface.

Carboxylic acids form one of the largest classes of stabilizers. The most pronounced effect is attained when the carboxylic acid molecules contain a long-chain hydrocarbon substituent which prevents agglomeration of particles. Among carboxylic acids, oleic acid is one of the best stabilizers.

Phosphonic acids have the general formula $OPR(OH)_2$, where R is a long-chain organic substituent. They differ from carboxylic acids in ability to form a stronger bond with cations from the nanocrystal lattice. Therefore, by varying the carboxylic-to-phosphonic acid ratio in the mixture one can change the surface energy of a nanocrystal.

Trioctylphosphine oxide is one of the most widely used cationic stabilizers which also often plays the role of a coordinating solvent.

Diols are a rarely used class of cationic stabilizers. Usually, they are used in combination with other classes of stabilizers.

Phosphines represent the most abundant type of anionic stabilizers. Relatively strong bonds between the phosphorus atoms and chalcogene atom (surface atom) allows one to passivate the broken bonds at chalcogene (these bonds act as traps for photoexcited holes). As a rule, passivation is achieved by introducing phosphines into the growth medium. A similar effect is also observed when using trioctylphosphine chalcogenides or tributylphosphine chalcogenides as initial reactants.

There are three general approaches to the synthesis, namely, successive 'buildup' of the shell from anionic and cationic components; cation exchange; and continuous growth of the shell on the core surface.

2. Successive shell growth

The successive ionic layer adsorption and reaction (SILAR) approach was the first method of synthesis of core/shell nanoparticles from cationic and anionic components.[75, 125] In essence, this is a layer-by-layer buildup of the shell. The SILAR method for the synthesis of nanoparticles is analogous to the molecular deposition method considered by Aleskovskii[126] and used for the synthesis of planar structures, *e.g.*, $A^{II}B^{VI}$ superlattices.[127] The state of the art in the field of research on the molecular deposition reactions was reviewed.[128] In the case of core/shell nanoparticles, molecular deposition is carried out in colloidal solutions. For instance, some calculated amounts of initial reactants (sources of cadmium and selenium) were added one at a time to a CdTe nanoparticle sol thoroughly purified from other cadmium and tellurium compounds.[75] The addition of the source of cation or anion was followed by heat treatment until total deposition of the whole amount of the initial reactant. The growth was controlled by optical and photoluminescence spectroscopies. The next portion of an initial reactant (source of selenium or cadmium) was added only after no red shift due to an increase in the particle size was observed in the spectra. Four CdSe monolayers were grown using this technique.

The development of the SILAR method is due to the need for elaboration of a high-precision shell buildup procedure to be used for the synthesis of core/shell nanoparticles with narrow size distribution and exactly specified shell thickness.[75] Also, this method is interesting for isotropic shell growth because it allows one to completely eliminate the effect of different growth rates along different crystallographic directions. A successful application of the SILAR method to the CdSe/CdS system was reported.[129]

3. Cation exchange

In ionic nanoparticles, in particular, transition metal chalcogenides, the cation sublattice can be replaced by various metal ions as a result of fast reversible cation exchange.[130] This affects the composition of nanoparticles but their size and shape remain unchanged.[130–135]

The cation exchange mechanism is as follows. The addition of the source of some other metal (*e.g.*, $AgNO_3$ solution in methanol) to the nanoparticles of a given binary semiconductor (*e.g.*, CdSe sol in toluene) causes an exchange in the cation sublattice, *i.e.*, Ag^+ cations replace Cd^{2+} cations but the anion sublattice remains unchanged (Fig. 19 *a*). This exchange is driven by the thermodynamic energy gain and different solubility of reactants and reaction products, because methanol forms stronger bonds with the doubly rather than singly charged cations.[130] The reaction proceeds at room temperature.[133] The reverse reaction (replacement of silver ions by cadmium ones) does not occur under similar conditions. However, the reverse cation exchange was practically implemented[130] upon a 100-fold increase in the concentration of the double-charged cation (Cd^{2+}) to be inserted and the addition of TBP to the reaction mixture (TBP is assumed to form intermediate complexes as ligand with initial reactant cati-

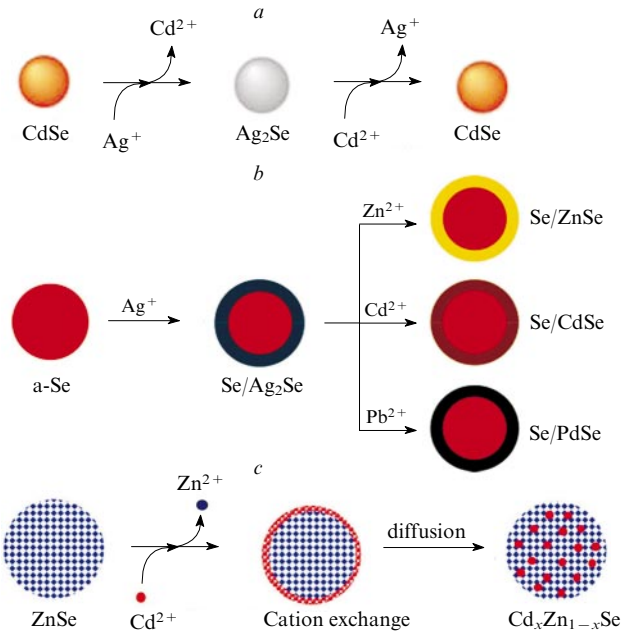


Figure 19. Scheme of cation exchange (*a*),[130] cation insertion followed by exchange (*b*)[133] and exchange of doubly charged cations (*c*).[135]

ons and these complexes facilitate the replacement of Ag^+ by Cd^{2+}).[130, 132, 133]

This approach was successfully employed for cation exchange $CdS \rightarrow Ag_2S$,[130, 132] $CdSe \rightarrow Ag_2Se$,[130] $CdTe \rightarrow Ag_2Te$,[130] $CdS \rightarrow Cu_2S \rightarrow PbS$,[131, 134] $CdSe \rightarrow Cu_2Se \rightarrow PbSe$,[134] and $Ag_2Se \rightarrow ZnSe$, CdSe or PbSe.[133] Conservation of the anion sublattice in the course of cation exchange enables transformations of multicomponent nanoparticles with conservation of not only the size and shape, but also the component ratio. This allows one to extend the field of application of the cation exchange method to the synthesis of core/shell nanoparticles.[132, 134] Cadmium cations can be completely exchanged by copper cations in the nanoparticles based on CdSe/CdS nanorods.[134] The exciton absorption bands characteristic of the CdSe nanoparticles disappear and a structureless absorption edge characteristic of copper chalcogenides appears. After the reverse reaction (replacement of copper ions by cadmium ones), peculiar features of the absorption spectra are recovered.[134]

A method[133] of preparation of Se/Ag_2Se nanoparticles is more similar to insertion of cations rather than cation exchange because the core is formed by amorphous selenium nanoparticles. A dropwise addition of a solution of $AgNO_3$ in ethylene glycol to a-Se nanoparticle sol over a period of 10 min led to a noticeable change in the colour of the sol. Then, the mixture was allowed to stay at room temperature for 2 h, nanoparticles were precipitated with water, washed and dissolved in methanol. The nanoparticles thus obtained were involved in cation exchange using a method analogous to that reported in Ref. 130. This technique was used to obtain Se/ZnSe, Se/CdSe and Se/PbSe nanoparticles (Fig. 19 *b*).

An alternative approach to cation exchange involves high-temperature treatment of nanoparticles in a solution of a precursor of the second cation.[135] Depending on the degree of cation exchange, three different systems can form, *viz*., nanoparticles based on the solid solution of the components, completely substituted nanoparticles and core/shell nanoparticles (Fig. 19 *c*).

4. Shell growth on nanoparticle seeds

Core/shell nanoparticles are also synthesized by a method without separation of the growth of anion and cation layers in time. A rather low supersaturation is produced instead to allow epitaxial growth of the shell on the surface of core type nanoparticles (they play the role of seeds) but to prevent nucleation of individual nanoparticles of the shell material.

One of the first one-step implementations of this method of synthesis of CdSe/ZnS nanoparticles was carried out using organometallic compounds as initial reactants.[136] First, CdSe nanoparticles were synthesized by introducing a dimethylcadmium solution and (TOP)Se in TOPO at 350 °C. When the reaction temperature decreased to 300 °C, a mixture of Me_2Zn and $(TMS)_2S$ in trioctylphosphine was added slowly to the solution. The temperature was maintained at 300 °C to prevent the formation of ZnS nanoparticles. As the whole amount of the mixture was added, the solution was cooled to 100 °C and allowed to stay at this temperature for 1 h.

A two-step modification[137] of this method involves isolation, purification and subsequent redispersion of the synthesized CdSe nanoparticles in hexane. Separation of the syntheses of the core type nanoparticles and core/shell nanoparticles allows one to remove residual amounts of initial reactants that did not react in the synthesis of the core type particles. The second important advantage of the two-step synthesis is the possibility of characterization of nanoparticle seeds, determination of their sizes, quantum photoluminescence yield, *etc*. Subsequently, an analogous method was used to synthesize CdSe/CdS,[138] CdSe/ZnS[139] and CdSe/ZnTe nanoparticles.[7]

V. Anisotropic nanoparticles with semiconductor/semiconductor heterojunctions

1. Growth of anisotropic $A^{II}B^{VI}$ and $A^{III}B^{V}$ semiconductor nanoparticles

Methods of synthesis of anisotropic $A^{II}B^{VI}$ and $A^{III}B^{V}$ nanoparticles are based on growth along a specified direction and branching.

The growth anisotropy can be manifested by various crystallographic structures. The presence of a specified growth direction in the wurtzite structure characteristic of many $A^{II}B^{VI}$ semiconductors is particularly pronounced. Owing to its high symmetry the wurtzite *c* axis differs from other growth directions. In the case of cadmium chalcogenide nanoparticles, the *c* axis can be used as the fast growth direction to obtain structures extended along this direction if an appropriate stabilizer has been chosen.[140] For example, CdSe nanorods grow as the wurtzite structure, which is confirmed by the results of X-ray diffraction and high-resolution transmission electron microscopy studies.[141] An array of vertically aligned rods that form a honeycomb structure was prepared.[141] Hexagonal faceting was observed for each rod. It should be noted that the wurtzite structure is more preferable for thin nanorods even under the conditions where the bulk material would exists as a zinc-blende structure; this is explained by a smaller number of broken bonds on the surface.[142, 143]

Branched nanoparticles are more complex objects. An interesting representative of such structures is a tetrapod, a four-legged design, each leg projecting from the centre at the tetrahedral angle (Fig. 20). All four legs are equivalent; therefore, the tetrapod is a highly symmetrical object belonging to the symmetry group T_d. Nanoparticles with tetrapod symmetry were obtained for a number of $A^{II}B^{VI}$ semiconductors including CdS,[144] CdSe,[145, 146] CdTe,[99] ZnO,[147] ZnS[148] and ZnSe.[149] A distinctive feature of some of these materials consists in that they are characterized by intermediate degrees of bond ionicity, which makes it

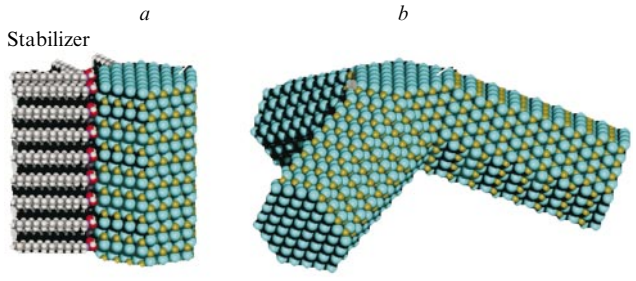


Figure 20. Schematic view of a tetrapod.[99]
Core face with sphalerite structure (*a*) and arm face with wurtzite structure (*b*). Lateral surface of tetrapod arm: shown are the molecules of stabilizer.

possible to form two types of crystal structures (polytypism). By and large, the growth mechanisms of tetrapods are close to those of nanorods, *viz*., the monomer is mainly deposited on high-energy end faces, whereas deposition of the monomer on lateral faces occurs more slowly. It is assumed that nucleation results in the formation of a core with the zinc-blende structure. Tetrapod legs grow selectively on the (111) face of the zinc-blende structure which is identical to the $(000\bar{1})$ face of the wurtzite structure.

Crystallographic faces of binary semiconductors have not only different densities of anions and cations, but can also be enriched with some sort of ions, *i.e*., they can be charged. For instance, in the wurtzite structure the (0001) face is built of cations, whereas the $(000\bar{1})$ face is comprised of anions while the plane families $\{01\bar{1}0\}$ and $\{11\bar{2}0\}$ are mixed, *i.e*. comprise cations and anions; therefore, they are electrically neutral, but the wurtzite structure is polar along the [0001] direction. Using methods of solution-phase synthesis, one can obtain anisotropic nanocrystals by varying the growth rates of different faces by changing the density of stabilizer molecules and the strength of their bonds with corresponding ions of the nanocrystal lattice. Therefore, there are two important characteristics of stabilizer molecules, namely, the selectivity and affinity to a certain face.[150, 151] It should be noted that the faces are characterized by different stabilities.[152]

A comparative analysis [152] of the stabilities and reactivities of different faces of the wurtzite polymorph of CdSe showed that the face of the $\{11\bar{2}0\}$ family is the most stable. Among polar faces, the anionic face $(000\bar{1})$ is the most stable under cadmium-deficiency conditions and the cationic face (0001) is the most stable under cadmium-rich conditions.

Adsorbed Se and Cd atoms are more strongly bound to the (0001) and $(000\bar{1})$ faces, respectively. On the one hand, binding the CdSe molecule to the (0001) surface with the molecule parallel to the crystal plane is more preferable. Rearrangement of the (0001) surface through the addition of the adsorbed atom favours a stronger binding of cadmium atoms and CdSe molecules and only slightly suppresses the binding of selenium atoms. On the other hand, the formation of a vacancy on the (0001) surface has no effect on the binding of cadmium atoms, but completely suppresses the adsorption of selenium atoms. Therefore, one can expect acceleration of growth of the (0001) face upon attachment of the adsorbed metal atom and suppression of growth in the presence of a vacancy.

Dissociation of CdSe molecules from all faces except $(000\bar{1})$ is an endothermic process; desorption from the $(000\bar{1})$ face is energetically favourable.[152] Moreover, among the faces investigated in Ref. 152, it is the $(000\bar{1})$ face for which sorption and sorption with subsequent dissociation are preferable. This is confirmed by a known hypothesis [97, 106, 107] according to which homoepitaxial growth is more favourable on the anionic face of the crystal.

Taking the wurtzite-type polymorph of CdSe as an example, the selectivities and affinities of some ligands to a nonpolar face from the $\{11\bar{2}0\}$ family, the $(000\bar{1})$ anionic face and the free and reduced (0001) cationic face were analyzed.[150, 151] Ligands included substances from the main classes of stabilizers which are currently used for the synthesis of nanoparticles in nonpolar solvents (Table 4).

Table 4. Model ligands and ligands used in the synthesis of CdSe nanocrystals.[150]

Ligand		Nanocrystal shape	Precursor concentration
model	experiment		
PH_3	trioctylphosphine	sphere	low
	tributylphosphine	rod	high
NH_3	oleylamine	sphere	low
OPH_3	trioctylphosphine oxide	"	"
	"	rod	high
HCOOH	oleic acid	sphere	low
OPH_2OH	hexadecylphosphinic acid		
	high concentration	rod	high
	low concentration	sphere	"

Among all ligands investigated,[150] only phosphine mainly binds to the $(000\bar{1})$ face. For other ligands, the bond stabilities increase in the series

$$OPH_3 < HCOOH < OPH_2OH < NH_3 < PH_3 .$$

In the case of the nonpolar face of the $\{11\bar{2}0\}$ family, the bond stability changes in the following series of ligands

$$PH_3 < OPH_3 < HCOOH < NH_3 < OPH_2OH.$$

The stabilities of the bonds between ligands and the polar cationic face (0001) vary in a similar fashion. Qualitatively, the interaction of ligands with these faces can be characterized as follows:

— PH_3 has a high affinity and selectivity to the $(000\bar{1})$ face,

— NH_3 has a high affinity and low selectivity to the face from the $\{11\bar{2}0\}$ family,

— OPH_3 has a moderate affinity and high selectivity to the face from the $\{11\bar{2}0\}$ family,

— HCOOH has a moderate affinity and high selectivity to the face from the $\{11\bar{2}0\}$ family,

— OPH_2OH has a high affinity and selectivity to the face from the $\{11\bar{2}0\}$ family.

High bond strength and high selectivity of OPH_2OH to the face from the $\{11\bar{2}0\}$ family favour its effective anisotropic growth in the kinetically controlled regime. This phenomenon was observed experimentally, namely, phosphonic acids are often used for the synthesis of nanorods. At the same time, bulk trialkylphosphine ligands modeled by PH_3 are mainly adsorbed with a low coverage and, as a consequence, they cannot favour anisotropic growth of the $(000\bar{1})$ anionic face in spite of high affinity and selectivity to this face. This is the reason for the use of trialkylphosphines in the synthesis of spherical nanoparticles.[89, 153, 154] Ligands with moderate binding energy, such as phosphine oxides and carboxylic acids, can also be used for the synthesis of spherical nanoparticles.

Among the ligands studied in Ref. 150, a specific position is occupied by amines that are characterized by high affinity but low selectivity to the anionic and cationic faces $(000\bar{1})$ and (0001), respectively. This combination of

properties allows amines to be used when growth of both polar faces is needed, *e.g.*, in the synthesis of dumbbell-shaped nanoparticles.[94]

As a rule, the shape of a crystal is determined by the growth rate difference between its faces. Similarly to the entire crystal, the growth rate of a particular face is determined by the concentrations of initial reactants near the growth surface and by the specific surface energy. The surface energies of the $A^{II}B^{VI}$ semiconductors in different crystallographic directions can be significantly different, although it to a great extent depends on the choice of stabilizer.[150, 151, 155]

The method of synthesis of anisotropic nanoparticles involving selective passivation of various faces cannot be adapted to semiconductor nanoparticles with cubic structure because of the lack of surfaces with marked chemical differences. Therefore, $A^{III}B^{V}$ semiconductors are synthesized using other approaches. A method was proposed of the synthesis of $A^{III}B^{V}$ semiconductor nanorods with high degree of crystallinity using metallic nanoparticles promoting one-directional growth.[156] This method is analogous to a widely used 'vapour – liquid – crystal' method of synthesis of whiskers using supported molten metal microdrops. The method allows one to obtain particles of variable length, in wide range. [156]

2. Synthesis of anisotropic nanoparticles with semiconductor/semiconductor heterojunction

The synthesis of anisotropic nanoparticles with semiconductor/semiconductor heterojunction can be practically implemented both under conditions of anisotropic growth of the second semiconductor material on spherical nanoparticles and under growth on anisotropic nanoparticles (Figs 21, 22).

The first approach is described in Refs 94, 95, 100, 105, 157. Various growth patterns of the arms of wurtzite-type $A^{II}B^{VI}$ semiconductors (CdS, CdSe, CdTe) on zinc-blende type seed nanoparticles (CdSe, CdTe, ZnTe) were demonstrated;[95] they allow one to obtain tetrapod morphology (see Fig. 21). It should be noted that in the tetrapods thus obtained both core and arms are built of CdTe. This two-step method of arm growth on seed nanoparticles is an alternative to the one-step methods of synthesis of CdTe tetrapods.[96, 99, 102] The possibility of obtaining nanoparticles comprising the $A^{II}B^{VI}$ and $A^{III}B^{V}$ semiconductor blocks was suggested.[95] Also, the possibility of control of nanoparticle morphology by varying the crystal structure of seed nanoparticles was reported.[100] It was shown that fast anisotropic growth of CdS arms on wurtzite-type CdSe seed nanoparticles leads to formation of nanorods; the growth on zinc-blende type CdSe nanoparticles results in tetrapods (see Fig. 22). Directed growth of CdS and CdTe arms on wurtzite-type CdTe and CdSe cores was realized by multiple injection of initial reactants.[94] This resulted in CdS/CdTe/CdS and CdTe/CdSe/CdTe nanorods with optical properties characteristic of nanoparticles with spatial separation of charge carriers. The size effect of the seed nanoparticles on the arm growth direction and morphology of final nanoparticles was revealed.[158]

A particular class is formed by anisotropic nanoparticles with semiconductor/metal CdSe/Au heterojunction;[159] they have an analogue of a contact pad for integration into conducting devices. Such nanoparticles are of interest for nanoelectronics.

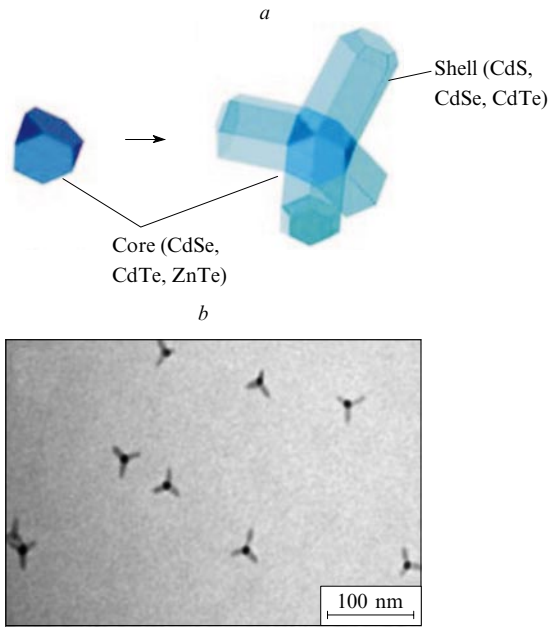


Figure 21. Scheme (*a*) and micrograph (*b*) of nanoparticles obtained by anisotropic growth of arms with wurtzite structure on nanoparticle seeds with sphalerite structure.[95]

The second approach to the synthesis of anisotropic nanoparticles comprising blocks of different materials implies growth on anisotropic seed nanoparticles, *e.g.*, nanorods or tetrapods, as was demonstrated in Ref. 98. The authors proposed a method of control of selective growth and the degree of branching of the material of the second semiconductor which makes it possible to specify the nanoparticle topology (Fig. 23).

Methods of control of the degree of anisotropy for multicomponent semiconductor nanoparticles are similar to the methods used in the synthesis of monocomponent nanoparticles. For instance, the effect of oleic acid concentration on the growth direction of CdSe arms in CdTe/CdSe nanoparticles based on CdTe tetrapods was demonstrated.[83, 103, 104, 160] Growth of CdSe arms using cadmium oleate as the source of cation and the ratio [Cd] : [oleic acid] = 1 : 2 proceeded selectively on the end face of an arm of CdTe tetrapod along the [0001] direction. At the ratio [Cd] : [oleic acid] = 1 : 3, the presence of free oleic acid in the reaction mixture led to passivation of the end cationic faces of the arms of CdTe tetrapod and blockage of growth along this direction. Concentric growth of CdSe shell on the lateral surface of the arms of CdTe tetrapods was observed instead.

Most methods of growth of anisotropic nanoparticles based on $A^{II}B^{VI}$ semiconductors allow one to obtain nanoparticles comprised of blocks of nanorods and tetrapods; this is due to the symmetry of the crystal structures of these materials (zinc-blende and wurtzite type). However, CdSe/CdS octapods were also prepared by combining the growth on seed nanoparticles and cation exchange.[161]

The most important difference of the optical properties of anisotropic nanoparticles with spatial separation of charge carriers from the optical properties of spherically symmetric core/shell nanoparticles is the emergence of internal field due to the spatial separation of charge

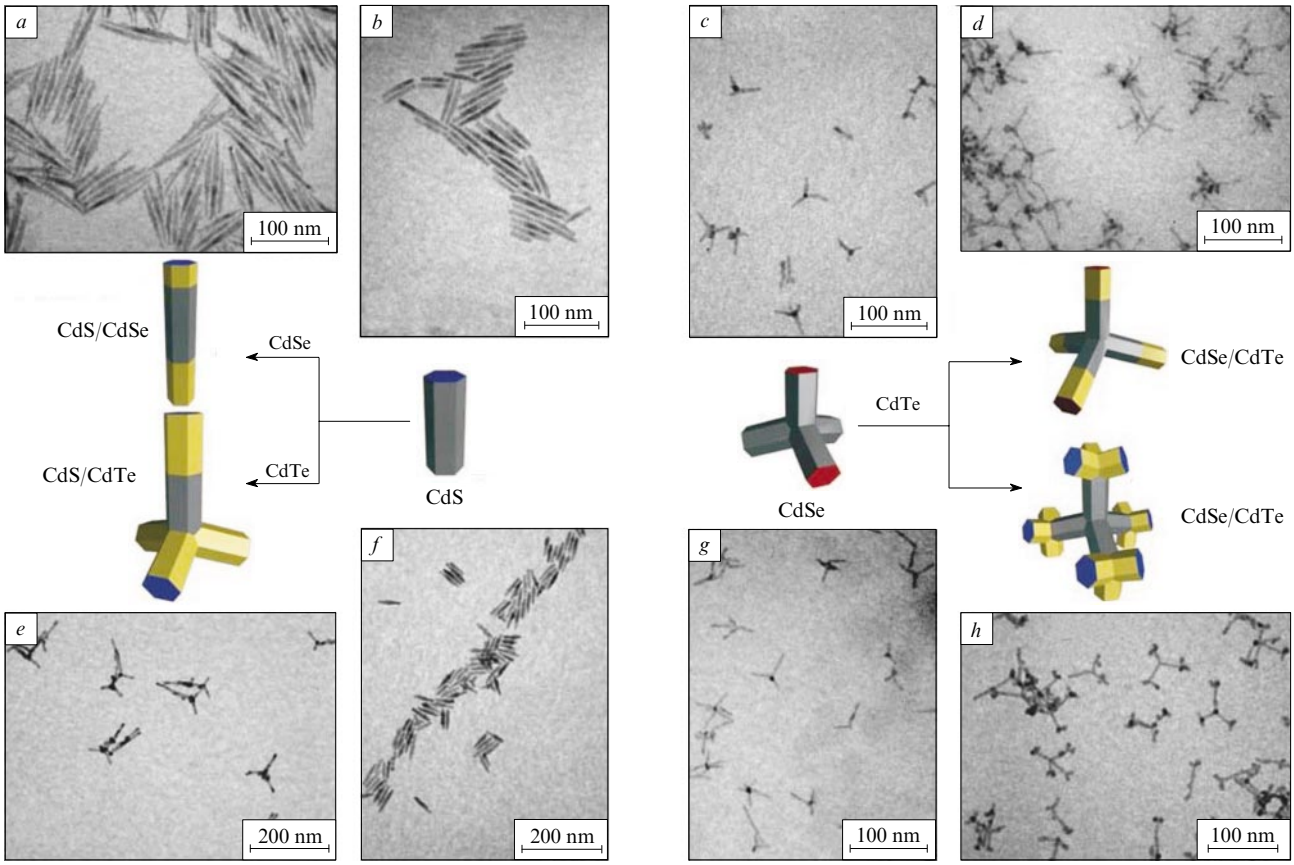


Figure 22. Schemes and micrographs of nanoparticles obtained by anisotropic growth of the second semiconductor domain on nanorods (*a*, *b*, *e*, *f*) and tetrapods (*c*, *d*, *g*, *h*).[98]

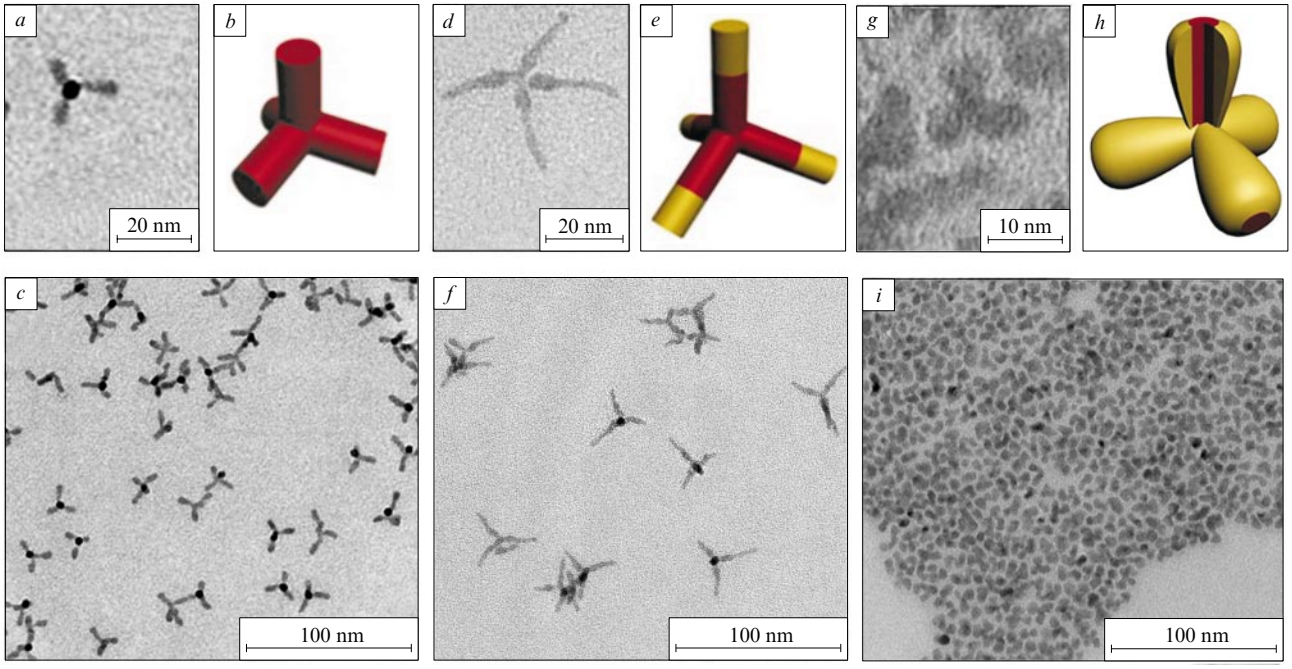


Figure 23. Tetrapod-shaped CdTe nanoparticles (*a*–*c*); CdTe/CdSe nanoparticles based on CdTe tetrapods, obtained at [Cd] : [oleic acid] = 1 : 2 (*d*–*f*); and CdTe/CdSe nanoparticles based on tetrapods CdTe, obtained at [Cd] : [oleic acid] = 1 : 3 (*g*–*i*).[83, 103, 104, 160]

carriers.[162] In particular, this leads to a strong dependence of the optical properties of such nanoparticles on the external electric field and on the degree of anisotropy because both these parameters affect the overlap integral of the electron and hole wave functions.[157, 163] Also, the influence of the temperature and nature of solvent on the separation of charge carriers in CdSe/CdTe anisotropic nanorods was reported.[164] The optical properties of anisotropic nanoparticles can be studied not only from the standpoint of the energy band structure of solids, but also from the standpoint of the Markus–Hush theory of charge transfer.[76, 81, 82, 165]

VI. Conclusion

The data presented in this review suggest that nanoparicles consisting of two and more epitaxially joined semiconductor fragments offer great prospects for control of their electronic properties. Such nanoparticles are characterized by pronounced quantum size effects. These systems occupy an intermediate position between charge-transfer molecular complexes and semiconductor heterostructures. The presence of junction between semiconductors allows one to control the spatial localization of photoexcited charges by both 'confinement' of the electron–hole pair in a certain fragment of the nanoparticle and 'separation' of photoexcited electron and hole in different parts of nanoparticles. This makes it possible to independently control the optical properties, namely, to specify the spectral positions of the absorption and luminescence bands, recombination times of the electron–hole pair and extinction coefficients.

Core/shell nanoparticles exhibit unique optical properties, *viz*., giant extinction coefficients (to 10^8 litre mol^{-1} cm^{-1}) and polarized luminescence. Luminescence can be controlled by varying the applied electric field. This can be of great importance for the design of solar cells, memory devices, laser media and biological labels.

Modern chemical methods allow one to synthesize semiconductor nanoparticles of specified size, composition and shape simultaneously with narrow particle size distribution and high shape homogeneity. One can expect that the development of methods of synthesis (especially, in order to obtain anisotropic nanoparticles with specified shape), as well as studies of electronic processes at the heterojunction will extend the possibilities of application of semiconductor nanoparticles in optoelectronics, biology and medicine.

This review has been written with partial financial support from the Federal Target Programme 'Research and Development in the Priority Areas of the Russian Science and Technology. Years 2007–2012' (Contract No. 16.516.11.8071).

Referenses

1. A P Alivisatos *Science* **271** 933 (1996)
2. M Achermann, M A Petruska, D D Koleske, M H Crawford, V I Klimov *Nano Lett*. **6** 1396 (2006)
3. P O Anikeeva, J E Halpert, M G Bawendi, V Bulovic *Nano Lett*. **7** 2196 (2007)
4. I Gur, N A Fromer, M L Geier, A P Alivisatos *Science* **310** 462 (2005)
5. R Costi, A E Saunders, E Elmalem, A Salant, U Banin *Nano Lett*. **8** 637 (2009)
6. *Semiconductor and Metal Nanocrystals: Synthesis and Electronic and Optical Properties* (Ed. V I Klimov) (New York: Marcel Dekker, 2004)
7. S Kim, B Fisher, H-J Eisler, M Bawendi *J. Am. Chem. Soc*. **125** 11466 (2003)
8. A Piryatinski, S A Ivanov, S Tretiak, V I Klimov *Nano Lett*. **7** 108 (2007)
9. *Molecular Beam Epitaxy and Heterostructures (NATO Science Series E)* (Eds. L L Chang, K Ploog) (New York: Springer, 1984)
10. V P Parini *Russ. Chem. Rev*. **31** 408 (1962)
11. G D Scholes *Adv. Funct. Mater*. **18** 1157 (2008)
12. P Reiss, M Protiere, L Li *Small* **5** 154 (2009)
13. Sh S Lo, T Mirkovic, Ch-H Chuang, C Burda, G D Scholes *Adv. Mater*. **23** 180 (2011)
14. L Carbone, P D Cozzoli *Nano Today* **5** 449 (2010)
15. C M Donega *Chem. Soc. Rev*. **40** 1512 (2011)
16. R Costi, A E Saunders, U Banin *Angew. Chem., Int. Ed*. **49** 4878 (2010)
17. A I Ekimov, A A Onushchenko *JETP Lett*. **34** 345 (1981)
18. R Rossetti, N Sakahara, L E Brus *J. Chem. Phys*. **79** 1086 (1983)
19. L Esaki *IEEE J. Quantum Electron*. **22** 1611 (1986)
20. Y Xia, P Yang, Y Sun, Y Wu, B Mayers, B Gates, Y Yin, F Kim, H Yan *Adv. Mater*. **15** 353 (2003)
21. Al L Efros, A L Efros *Fiz. Tekhn. Poluprovod*. **16** 1209 (1982) [a]
22. S Adachi *Properties of Group-IV, III–V and II–VI Semiconductors* (Chichester: Willey, 2005)
23. L Li, J Hu, W Yang, A P Alivisatos *Nano Lett*. **1** 349 (2001)
24. D Katz, T Wizansky, O Millo, E Rothenberg, T Mokari, U Banin *Phys. Rev. Lett*. **89** 086801 (2002)
25. C Burda, X Chen, R Narayanan, M A El-Sayed *Chem. Rev*. **105** 1025 (2005)
26. A I Ekimov, F Hache, M C Schanne-Klein, D Ricard, C Flytzanis, I A Kudryavtsev, T V Yazeva, A V Rodina, Al L Efros *J. Opt. Soc. Am. B* **10** 100 (1993)
27. U Banin, G Cerullo, A A Guzelian, C J Bardeen, A P Alivisatos, C V Shank *Phys. Rev. B* **55** 7059 (1997)
28. J Li, L-W Wang *Nano Lett*. **3** 1357 (2003)
29. M T Harrison, S V Kershaw, M G Burt, A L Rogach, A Kornowski, A Eychmüller, H Weller *Pure Appl. Chem*. **72** 295 (2000)
30. W W Yu, L Qu, W Guo, X Peng *Chem. Mater*. **15** 2854 (2003)
31. W W Yu, L Qu, W Guo, X Peng *Chem. Mater*. **16** 560 (2004)
32. V I Klimov *J. Phys. Chem. B* **104** 6112 (2000)
33. C M Donega, R Koole *J. Phys. Chem*. **113** 6511 (2009)
34. L E Brus *J. Chem. Phys*. **80** 4403 (1984)
35. T Rajh, O I Micic, A J Nozik *J. Phys. Chem*. **97** 11999 (1993)
36. S Adam, D V Talapin, H Borchert, A Lobo, C McGinley, A R B de Castro, M Haase, H Weller, T Moller *J. Chem. Phys*. **123** 084706 (2005)
37. J Jasieniak, L Smith, J Embden, P Mulvaney, M Califano *J. Phys. Chem. C* **113** 19468 (2009)
38. T Vossmeyer, L Katsikas, M Giersig, I G Popovic, K Diesner, A Chemseddine, A Eychmüller, H Weller *J. Phys. Chem*. **98** 7665 (1994)
39. P Yu, M C Beard, R J Ellingson, S Ferrere, C Curtis, J Drexler, F Luiszer, A J Nozik *J. Phys. Chem. B* **109** 7084 (2005)
40. C A Leatherdale, W-K Woo, F V Mikulec, M G Bawendi *J. Phys. Chem. B* **106** 7619 (2002)
41. E Kucur, F M Boldt, S Cavaliere-Jaricot, J Ziegler, Th Nann *Anal. Chem*. **79** 8987 (2007)
42. O Schmelz, A Mews, Th Basche, A Herrmann, K Mullen *Langmuir* **17** 2861 (2001)

43. A Striolo, J Ward, J M Prausnitz, W J Parak, D Zanchet, D Gerion, D Milliron, A P Alivisatos *J. Phys. Chem. B* **106** 5500 (2002)
44. S Adachi, T Kimura, N Suzuki *J. Appl. Phys.* **74** 3435 (1993)
45. S Ninomiya, S Adachi *J. Appl. Phys.* **78** 4681 (1995)
46. S Ninomiya, S Adachi *J. Appl. Phys.* **78** 1183 (1995)
47. S-H Wei, S B Zhang *Phys. Rev. B* **62** 6944 (2000)
48. S Sanguinetti, T Mano, M Oshima, T Tateno, M Wakaki, N Koguchi *Appl. Phys. Lett.* **81** 3067 (2002)
49. B N Littleton, M J Fernee, D E Gomez, P Mulvaney, G Rubinsztein-Dunlop *J. Phys. Chem. C* **113** 5345 (2009)
50. S Malkmus, S Kudera, L Manna, W J Parak, M Braun *J. Phys. Chem. B* **110** 17334 (2006)
51. F T Vasko, A V Kuznetsov *Electronic States and Optical Transitions in Semiconductor Heterostructures* (New York: Springer, 1999)
52. G Bastard *Wave Mechanics Applied to Semiconductor Heterostructures* (Les Ules Cedex: EDP Sciences, 1992)
53. *Semiconductor Surfaces and Interfaces* (Eds F Bechstedt, R Enderlein) (Berlin: Akademie-Verlag, 1988)
54. S A Ivanov, J Nanda, A Piryatinski, M Achermann, L P Balet, I V Bezel, P O Anikeeva, S Tretiak, V I Klimov *J. Phys. Chem. B* **108** 10625 (2004)
55. V I Klimov, S A Ivanov, J Nanda, M Achermann, I Bezel, J A McGuire, A Piryatinski *Nature (London)* **447** 441 (2007)
56. L P Balet, S A Ivanov, A Piryatinski, M Achermann, V I Klimov *Nano Lett.* **4** 1485 (2004)
57. J Nanda, S A Ivanov, H Htoon, I Bezel, A Piryatinski, S Tretiak, V I Klimov *J. Appl. Phys.* **99** 034309 (2006)
58. C G Van de Walle, J Neugebauer *Nature (London)* **423** 626 (2003)
59. V A Kuznetsov *Fiz. Tekhn. Poluprovod.* **44** 1153 (2010) [a]
60. N I Vitryakhovskii, I B Mizetskaya *Fiz. Tv. Tela* **1** 397 (1959) [b]
61. N I Vitryakhovskii, A A Kipen', O V Mykhas'kin *Fiz. Tekhn. Poluprovod.* **6** 1193 (1975) [a]
62. S Balasubramanian, G Ceder, K D Kolenbrander *J. Appl. Phys.* **79** 4132 (1996)
63. A J Ardell, A Maheshwari *Acta Metall. Mater.* **43** 1825 (1995)
64. S Suresh, A E Giannakopoulos, M Olsson *J. Mech. Phys. Solids* **42** 979 (1994)
65. J D Eshelby *Proc. R. Soc. London, Ser. A* **241** 376 (1957)
66. N F Mott, F R N Nabarro *Proc. Phys. Soc.* **52** 86 (1940)
67. P W Voorhees, W C Johnson *J. Chem. Phys.* **84** 5108 (1986)
68. Ch G Van de Walle *Phys. Rev. B* **39** 1871 (1989)
69. Y Yamada, Y Masumoto, T Taguchi, K Takemura *Phys. Rev. B* **44** 1801 (1991)
70. S-H Wei, A Zunger *Phys. Rev. B* **60** 5404 (1999)
71. Y-H Li, X G Gong, S-H Wei *Phys. Rev. B* **73** 245206 (2006)
72. A M Smith, A M Mohs, Sh Nie *Nature Nanotechnol.* **4** 56 (2009)
73. A Smith, Sh Nie *Acc. Chem. Res.* **43** 190 (2010)
74. C L Yuan, H Cai, P S Lee, J Guo, J He *J. Phys. Chem. C* **113** 19863 (2009)
75. J J Li, J M Tsay, X Michalet, Sh Weiss *Chem. Phys.* **318** 82 (2005)
76. M Jones, S Kumar, S S Lo, G D Scholes *J. Phys. Chem. C* **112** 5423 (2008)
77. D Oron, M Kazes, U Banin *Phys. Rev. B* **75** 035330 (2007)
78. S A Ivanov, A Piryatinski, J Nanda, S Tretiak, K R Zavadil, W O Wallace, D Werder, V I Klimov *J. Am. Chem. Soc.* **129** 11708 (2007)
79. Ö Schops, N Le Thomas, U Woggon, M V Artemyev *J. Phys. Chem. B* **110** 2074 (2006)
80. G D Scholes, M Jones, S Kumar *J. Phys. Chem. C* **111** 13777 (2007)
81. C J Dooley, S D Dimitrov, T Fiebig *J. Phys. Chem. C* **112** 12074 (2008)
82. A D Yoffe *Adv. Phys.* **50** 1 (2001)
83. R B Vasiliev, D N Dirin, M S Sokolikova, V V Roddatis, A L Vasiliev, A G Vitukhnovsky, A M Gaskov *J. Mater. Res.* **26** 1621 (2011)
84. Al L Efros, M Rosen, M Kuno, M Nirmal, D J Norris, M Bawendi *Phys. Rev. B* **54** 4843 (1996)
85. G Markovich, C P Collier, S E Henrich, F Remacle, R D Levine, J R Heath *Acc. Chem. Res.* **32** 415 (1999)
86. M L Steigerwald, L E Brus *Annu. Rev. Mater. Sci.* **19** 471 (1989)
87. C P Collier, T Vossmeyer, J R Heath *Annu. Rev. Phys. Chem.* **49** 371 (1998)
88. M G Bawendi, A R Kortan, M L Steigerwald, L E Brus *J. Chem. Phys.* **91** 7282 (1989)
89. C B Murray, D J Norris, M G Bawendi *J. Am. Chem. Soc.* **115** 8706 (1993)
90. Y Yin, A P Alivisatos *Nature (London)* **437** 664 (2005)
91. X Peng, J Wickham, A P Alivisatos *J. Am. Chem. Soc.* **120** 5343 (1998)
92. J Park, J Joo, S G Kwon, Y Jang, T Hyeon *Angew. Chem., Int. Ed.* **46** 4630 (2007)
93. R B Vasiliev, S G Dorofeev, D N Dirin, D A Belov, T A Kuznetsova *Mendeleev Commun.* 169 (2004)
94. F Shieh, A E Saunders, B A Korgel *J. Phys. Chem. B* **109** 8538 (2005)
95. A Fiore, R Mastria, M G Lupo, G Lanzani, C Giannini, E Carlino, G Morello, M De Giorgi, Y Li, R Cingolani, L Manna *J. Am. Chem. Soc.* **131** 2274 (2009)
96. W W Yu, Y A Wang, X Peng *Chem. Mater.* **15** 4300 (2003)
97. Z A Peng, X Peng *J. Am. Chem. Soc.* **124** 3343 (2002)
98. D J Milliron, S M Hughes, Y Cui, L Manna, J Li, L-W Wang, A P Alivisatos *Nature (London)* **430** 190 (2004)
99. L Manna, D J Milliron, A Meisel, E C Scher, A P Alivisatos *Nature Mater.* **2** 382 (2003)
100. D V Talapin, J H Nelson, E V Shevchenko, Sh Aloni, B Sadtler, A P Alivisatos *Nano Lett.* **7** 2951 (2007)
101. L H Qu, Z A Peng, X G Peng *Nano Lett.* **1** 333 (2001)
102. R B Vasiliev, D N Dirin, A M Gaskov *Mendeleev Commun.* **19** 126 (2008)
103. R B Vasiliev, D N Dirin, M S Sokolikova, S G Dorofeev, A G Vitukhnovsky, A M Gaskov *Mendeleev Commun.* **19** 128 (2008)
104. D N Dirin, R B Vasil'ev, M S Sokolikova, A M Gaskov *Neorg. Mater.* **47** 1 (2011) [c]
105. D V Talapin, R Koeppe, S Gotzinger, A Kornowski, J M Lupton, A L Rogach, O Benson, J Feldman, H Weller *Nano Lett.* **3** 1677 (2003)
106. Z A Peng, X Peng *J. Am. Chem. Soc.* **123** 1389 (2001)
107. L Manna, E C Scher, A P Alivisatos *J. Am. Chem. Soc.* **122** 12700 (2000)
108. D V Talapin, S Haubold, A L Rogach, A Kornowski, M Haase, H Weller *J. Phys. Chem. B* **105** 2260 (2001)
109. L Manna, E C Scher, L-Sh Li, A P Alivisatos *J. Am. Chem. Soc.* **124** 7136 (2002)
110. J G Brennan, T Siegrist, P J Carroll, S M Stuczynski, P Reynders, L E Brus, M L Steigerwald *Chem. Mater.* **2** 403 (1990)
111. A L Rogach, A Eychmüller, S G Hickey, S V Kershaw *Small* **3** 536 (2007)
112. D W Lucey, D J MacRae, M Furis, Y Sahoo, A N Cartwright, P N Prasad *Chem. Mater.* **17** 3754 (2005)
113. H S Nalwa *Handbook of Nanostructured Materials and Nanotechnology* Vol. 3 (San Diego, CA: Academic Press, 2000)
114. O I Micic, A J Nozik *J. Luminesc.* **70** 95 (1996)
115. R L Wells, S R Aubuchon, S S Kher, M S Lube, P S White *Chem. Mater.* **7** 793 (1995)
116. A A Guzelian, U Banin, A V Kadavanich, X Peng, A P Alivisatos *Appl. Phys. Lett.* **69** 1432 (1996)

117. A A Guzelian, J E B Katari, A V Kadavanich, U Banin, K Hamad, E Juban, A P Alivisatos, R H Wolters, C C Arnold, J R Heath *J. Phys. Chem.* **100** 7212 (1996)
118. O I Micic, J Sprague, Zh Lu, A J Nozik *Appl. Phys. Lett.* **68** 3150 (1996)
119. O I Micic, H M Cheong, H Fu, A Zunger, J R Sprague, A Mascarenhas, A J Nozik *J. Phys. Chem. B* **101** 4904 (1997)
120. D V Talapin, A L Rogach, I Mekis, S Haubold, A Kornowski, M Haase, H Weller *Colloids Surf., A* **202** 145 (2002)
121. O L Micic, J R Sprague, C J Curtis, K M Jones, J L Machol, A J Nozik, H Giessen, B Fluegel, G Mohs, N Peyghambarian *J. Phys. Chem.* **99** 7754 (1995)
122. O I Micic, C J Curtis, K M Jones, J R Sprague, A J Nozik *J. Phys. Chem.* **98** 4966 (1994)
123. D Battaglia, X Peng *Nano Lett.* **2** 1027 (2002)
124. E J W Verwey, J Th G Overbeek *Theory of the Stability of Lyophobic Colloids* (Amsterdam: Elsevier, 1948)
125. B Blackman, D M Battaglia, T D Mishima, M B Johnson, X Peng *Chem. Mater.* **19** 3815 (2007)
126. V B Aleskovskii *Zh. Prikl. Khim.* **47** 2145 (1974) [d]
127. D A Ageev, V B Aleskovskii, R A Bisengaliev, V I Gubaidullin, V E Drozd, B V Novikov, A P Savchenko *Fiz. Tv. Tela* **40** 820 (1998) [b]
128. V P Tolstoy *Russ. Chem. Rev.* **75** 161 (2006)
129. J J Li, Y A Wang, W Guo, J C Keay, T D Mishima, M B Johnson, X Peng *J. Am. Chem. Soc.* **125** 12567 (2003)
130. D H Son, S M Hughes, Y Yin, A P Alivisatos *Science* **306** 1009 (2004)
131. J M Luther, H Zheng, B Sadtler, A P Alivisatos *J. Am. Chem. Soc.* **131** 16851 (2009)
132. P Peng, B Sadtler, A P Alivisatos, R J Saykally *J. Phys. Chem. C* **114** 5879 (2010)
133. P H C Camargo, Y H Lee, U Jeong, Z Zou, Y Xia *Langmuir* **23** 2985 (2007)
134. P K Jain, L Amirav, S Aloni, A P Alivisatos *J. Am. Chem. Soc.* **132** 9997 (2010)
135. X Zhong, Y Feng, Y Zhang, Z Gu, L Zou *Nanotechnology* **18** 385606 (2007)
136. M A Hines, P Guyot-Sionnest *J. Phys. Chem.* **100** 468 (1996)
137. B O Dabbousi, J Rodriguez-Viejo, F V Mikulec, J R Heine, H Mattoussi, R Ober, K F Jensen, M G Bawendi *J. Phys. Chem. B* **101** 9463 (1997)
138. X Peng, M C Schlamp, A V Kadavanich, A P Alivisatos *J. Am. Chem. Soc.* **119** 7019 (1997)
139. D V Talapin, A L Rogach, A Kornowski, M Haase, H Weller *Nano Lett.* **1** 207 (2001)
140. G M Dalpian, M L Tiago, M L del Puerto, J R Chelikowsky *Nano Lett.* **6** 501 (2006)
141. X Peng, L Manna, W Yang, J Wickham, E Scher, A Kadavanich, A P Alivisatos *Nature (London)* **404** 59 (2000)
142. P Lawaetz *Phys. Rev. B* **5** 4039 (1972)
143. T Akiyama, K Nakamura, T Ito *Phys. Rev. B* **73** 235308 (2006)
144. Y-W Jun, S-M Lee, N-J Kang, J Cheon *J. Am. Chem. Soc.* **123** 5150 (2001)
145. Q Pang, L Zhao, Y Cai, D P Nguyen, N Regnault, N Wang, S H Yang, W Ge, R Ferreira, G Bastard, J Wang *Chem. Mater.* **17** 5263 (2005)
146. S Asokan, K M Krueger, V L Colvin, M S Wong *Small* **3** 1164 (2007)
147. K Nishio, T Isshiki, M Kitano, M Shiojiri *Philos. Mag. A* **76** 889 (1997)
148. Y-Ch Zhu, Y Bando, D-F Xue, D Golberg *J. Am. Chem. Soc.* **125** 16196 (2003)
149. J Hu, Y Bando, D Golberg *Small* **1** 95 (2005)
150. J Y Rempel, B L Trout, M G Bawendi, K F Jensen *J. Phys. Chem. B* **110** 18007 (2006)
151. A Puzder, A J Williamson, N Zaitseva, G Galli, L Manna, A P Alivisatos *Nano Lett.* **4** 2361 (2004)
152. J Y Rempel, B L Trout, M G Bawendi, K F Jensen *J. Phys. Chem. B* **109** 19320 (2005)
153. S F Wuister, C de Mello Donega, A Meijerink *J. Am. Chem. Soc.* **126** 10397 (2004)
154. P T Snee, Y Chan, D G Nocera, M G Bawendi *Adv. Mater.* **17** 1131 (2005)
155. A Puzder, A J Williamson, F Gygi, G Galli *Phys. Rev. Lett.* **92** 217401 (2004)
156. Sh Kan, A Aharoni, T Mokari, U Banin *Faraday Discuss.* **125** 23 (2004)
157. R M Kraus, P G Lagoudakis, A L Rogach, D V Talapin, H Weller, J M Lupton, J Feldmann *Phys. Rev. Lett.* **98** 017401 (2007)
158. H Zhong, G D Scholes *J. Am. Chem. Soc.* **131** 9170 (2009)
159. T Mokari, E Rothenberg, I Popov, R Costi, U Banin *Science* **304** 1787 (2004)
160. A G Vitukhnovsky, A S Shul'ga, S A Ambrozevich, E M Khokhlov, R B Vasiliev, D N Dirin, V I Yudson *Phys. Lett. A* **377** 2287 (2009)
161. S Deka, K Miszta, D Dorfs, A Genovese, G Bertoni, L Manna *Nano Lett.* **10** 3770 (2010)
162. G Morello, F D Sala, L Carbone, L Manna, G Maruccio, R Cingolani, M De Giorgi *Phys. Rev. B* **78** 195313 (2008)
163. J Müller, J M Lupton, P G Lagoudakis, F Schindler, R Koeppe, A L Rogach, J Feldmann, D V Talapin, H Weller *Nano Lett.* **5** 2044 (2005)
164. S S Lo, Y Khan, M Jones, G D Scholes *J. Chem. Phys.* **131** 084714 (2009)
165. J He, S S Lo, J Kim, G D Scholes *Nano Lett.* **8** 4007 (2008)

[a] — *Semiconductors (Engl. Transl.)*
[b] — *Phys. Solid State (Engl. Transl.)*
[c] — *Inorg. Mater. (Engl. Transl.)*
[d] — *Russ. J. Appl. Chem. (Engl. Transl.)*